REPORT

MEMORY RESEARCH

Engrams and circuits crucial for systems consolidation of a memory

Takashi Kitamura,[1]* Sachie K. Ogawa,[1]* Dheeraj S. Roy,[1]* Teruhiro Okuyama,[1] Mark D. Morrissey,[1] Lillian M. Smith,[1] Roger L. Redondo,[1,2]† Susumu Tonegawa[1,2]‡

Episodic memories initially require rapid synaptic plasticity within the hippocampus for their formation and are gradually consolidated in neocortical networks for permanent storage. However, the engrams and circuits that support neocortical memory consolidation have thus far been unknown. We found that neocortical prefrontal memory engram cells, which are critical for remote contextual fear memory, were rapidly generated during initial learning through inputs from both the hippocampal–entorhinal cortex network and the basolateral amygdala. After their generation, the prefrontal engram cells, with support from hippocampal memory engram cells, became functionally mature with time. Whereas hippocampal engram cells gradually became silent with time, engram cells in the basolateral amygdala, which were necessary for fear memory, were maintained. Our data provide new insights into the functional reorganization of engrams and circuits underlying systems consolidation of memory.

Memories are thought to be initially stored within the hippocampal–entorhinal cortex (HPC-EC) network (recent memory) and, over time, slowly consolidated within the neocortex for permanent storage (remote memory) (*1*–*7*). Systems memory consolidation models suggest that the interaction between the HPC-EC network and the neocortex during and after an experience is crucial (*8*–*12*). Experimentally, prolonged inhibition of hippocampal or neocortical networks during the consolidation period produces deficits in remote memory formation (*13*–*15*). However, little is known regarding specific neural circuit mechanisms underlying the formation and maturation of neocortical memories through interactions with the HPC-EC network. Using activity-dependent cell-labeling technology (*16*–*18*), combined with viral vector–based transgenic, anatomical (*19*, *20*), and optogenetic strategies (*19*, *21*) for circuit-specific manipulations and in vivo calcium imaging (*22*), we investigated the nature and dynamics of neocortical and subcortical memory engram cells [a population of neurons that are activated by learning, have enduring cellular changes, and are reactivated by a part of the original stimuli for recall (*18*)] and their circuits for systems consolidation of memory.

We first traced entorhinal projections to frontal cortical structures [the medial prefrontal cortex (PFC), caudal anterior cingulate cortex (cACC), and retrosplenial cortex (RSC)] involved in contextual fear memory, as well as to the basolateral amygdala (BLA), with injections of the retrograde tracer cholera toxin subunit B–Alexa*555* (hereafter, CTB injections) into these regions (fig. S1). CTB injections resulted in labeling in the medial entorhinal cortex (MEC), specifically in cells in layer Va (Fig. 1, A to D and H, and fig. S2, A to D), indicating that MEC-Va cells have extensive projections to the neocortex and BLA (*23*). We then sought to inhibit these specific projections by bilaterally injecting adeno-associated virus 8 (AAV_8)–calcium/calmodulin-dependent protein kinase II (CaMKII):eArchT–enhanced yellow fluorescent protein (eYFP) in the deep layers of the MEC in wild-type (WT) mice with bilaterally implanted optic fibers above the PFC, cACC, or RSC (Fig. 1, E and J, and fig. S2G). Expression of eArchT-eYFP was abundant in MEC-Va terminals located in each of these regions (Fig. 1, B and I, and fig. S2D). These mice were then subjected to contextual fear conditioning (CFC) while we delivered green light bilaterally to the different cortical areas that have MEC-Va projections during either the conditioning period (day 1) (fig. S2E) or the recall test period (days 2, 8, 15, and 22) (fig. S2F). Axon terminal inhibition with optogenetics of MEC-Va cells within the PFC during day 1 of CFC disrupted memory at days 15 and 22, but not at days 2 or 8 (Fig. 1F). Terminal inhibition during memory recall tests did not affect memory retrieval (Fig. 1G). Last, terminal inhibition in the cACC or RSC during CFC or recall had no effect on memory throughout these periods (Fig. 1, J to L, and fig. S2, G to I).

The above results suggest that MEC-Va input into the PFC during CFC is crucial for the eventual formation of remote memory. This hypothesis was supported by several findings. First, CFC increased the number of c-Fos^+ cells in the PFC compared with that in the PFC of home-cage mice (Fig. 1, M to O), whereas context-only exposure did not increase c-Fos activity in the PFC (Fig. 1O). Second, optogenetic terminal inhibition of MEC-Va projections within the PFC during CFC inhibited the observed increase of c-Fos^+ cells in the PFC (Fig. 1O). Last, we identified CFC engram cells in the PFC. We targeted injections of AAV_9–c-fos:tetracycline-controlled transactivator (tTA) and AAV_9–tetracycline response element (TRE):channelrhodopsin-2 (ChR2)–mCherry (Fig. 1, P and Q) and optic fibers to the PFC of WT mice and labeled the PFC cells activated by CFC with ChR2 while the mice were off doxycycline (Fig. 1R). Blue light stimulation at 4 Hz, but not at the conventional 20 Hz, of ChR2-mCherry–expressing cells in the PFC induced increased freezing behavior on days 2 and 12 in an unconditioned context (Fig. 1S and fig. S3), compared with freezing under the blue light–off condition. This blue light–induced freezing was prevented when MEC-Va fibers in the PFC were inhibited during CFC on day 1 (Fig. 1, T and U, and fig. S4). Using transsynaptic retrograde tracing combined with the activity-dependent cell labeling, we confirmed that the PFC engram cells generated by CFC received monosynaptic input from MEC-Va cells (Fig. 1, V to X, and fig. S5).

To examine whether PFC engram cells are also reactivated by the conditioned context (rather than by blue light) at recent and remote time points, we targeted injections of AAV_9-TRE:human histone H2B–green fluorescent protein (H2B-GFP) to the PFC of c-fos:tTA transgenic mice (Fig. 2A). The mice underwent CFC on day 1 and then were reexposed to the conditioned (context A) or an unconditioned (context B) context on days 2 or 13 (Fig. 2B). Cells activated by CFC were labeled with H2B-GFP, and the cells activated by the context test were labeled with a c-Fos antibody; we calculated the proportion of double-labeled cells (Fig. 2, A to B, and fig. S6B). Compared with H2B-GFP^- cells, H2B-GFP^+ cells (PFC engram cells) were preferentially reactivated in context A on day 13, but not on day 2 (Fig. 2C). There was no difference in c-Fos expression between H2B-GFP^+ and H2B-GFP^- cells when mice were tested in context B (Fig. 2C). We also found that the spine density of the PFC engram cells on day 12 was significantly higher than on day 2 (Fig. 2, D and E, and fig. S7), in line with previous findings of a positive correlation between the dendritic spine density of memory engram cells and memory expression triggered by natural recall cues (*24*–*26*).

To test whether PFC engram cells are necessary for memory recall by natural cues, we bilaterally targeted injections of AAV_9–c-fos:tTA and AAV_9-TRE:ArchT-eGFP (Fig. 2, D and F) and optic fibers to the PFC of WT mice and labeled the PFC engram cells that were activated by CFC with ArchT while the mice were off doxycycline (Fig. 2F). Cell body inhibition of the

[1]RIKEN-MIT Center for Neural Circuit Genetics at the Picower Institute for Learning and Memory, Departments of Biology and Brain and Cognitive Sciences, Massachusetts Institute of Technology, Cambridge, MA 02139, USA. [2]Howard Hughes Medical Institute, Massachusetts Institute of Technology, Cambridge, MA 02139, USA.
*These authors contributed equally to this work. †Present address: Roche Pharmaceutical Research and Early Development, Roche Innovation Center, F. Hoffmann-La Roche, Basel, Switzerland.
‡Corresponding author. Email: tonegawa@mit.edu

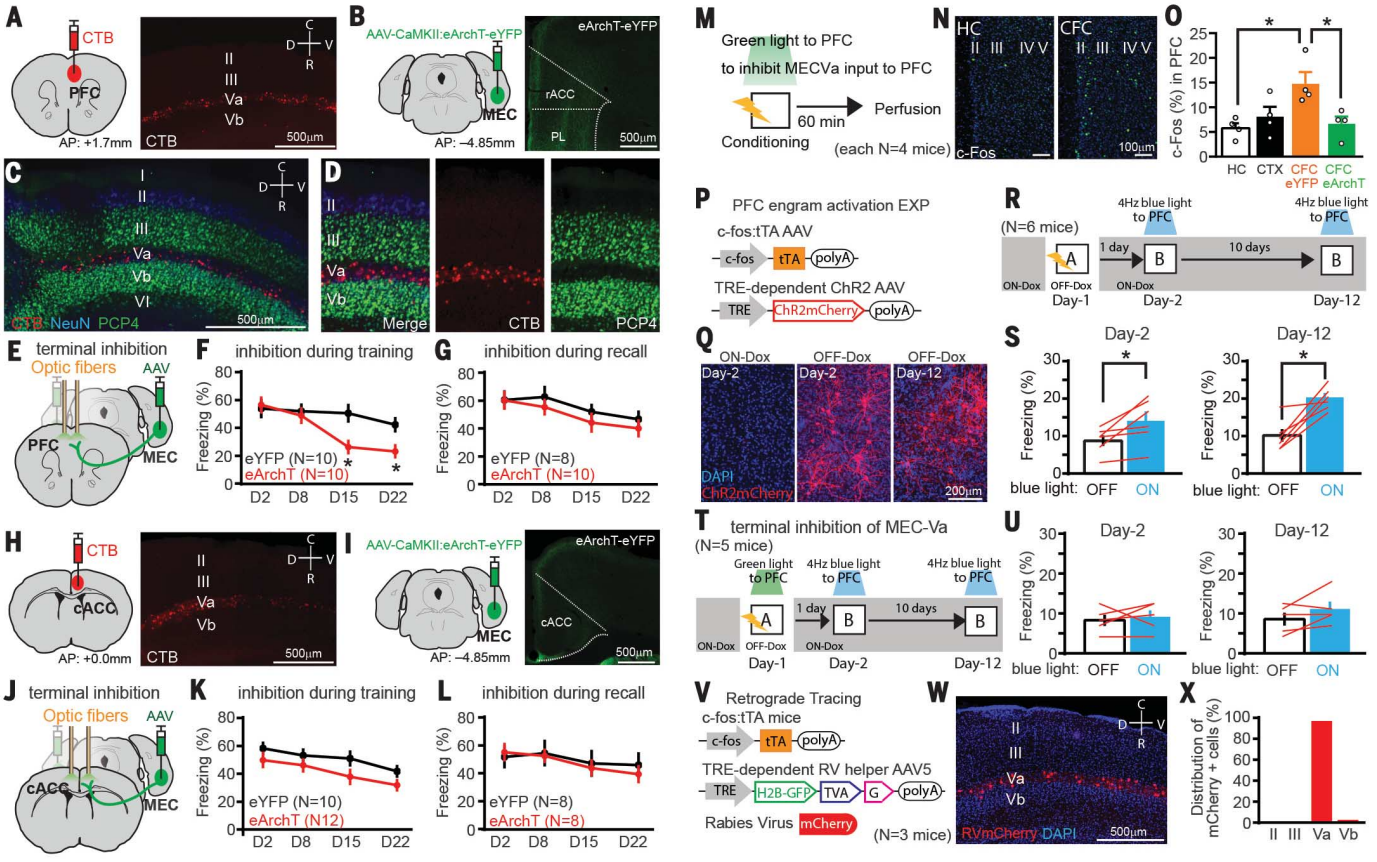

Fig. 1. MEC-Va input to the PFC during conditioning is crucial for generation of PFC engram cells. (**A**) CTB injection into the PFC (left) and sagittal section of the MEC with CTB-labeled cells (red) (right). AP, anterior posterior; C, caudal; R, rostral; D, dorsal; V, ventral. (**B**) AAV_8-CaMKII:eArchT-eYFP injection into the MEC (left) and coronal sections of PFC with MEC-Va axons expressing eYFP (green) (right). rACC, rostral ACC; PL, prelimbic cortex. (**C** and **D**) Sagittal section of MEC with CTB-labeled cells (red), immunostained with anti-PCP4 (green) and anti-NeuN (blue). PCP4 is a marker for layer III and Vb cells in MEC. The images were produced following CTB injection into the BLA. (**E** and **J**) Viral injections and optic fiber implantations. (**F** and **G**) Time courses (D, day) of freezing during recall tests. Green light was shone into the PFC during conditioning (F) or testing (G). (**H**) CTB injection into caudal ACC (cACC) (left) and sagittal section of the MEC with CTB-labeled cells (red) (right). (**I**) AAV_8-CaMKII:eArchT-eYFP injection into the MEC (left) and coronal sections of cACC with MEC-Va axons (green) (right). (**K** and **L**) Time courses of freezing during recall tests. Green light was shone into the cACC during conditioning (K) or testing (L). (**M**) Experimental schedule. (**N**) Coronal section of PFC with anti–c-Fos (green). HC, home cage; CFC, contextual fear conditioning. (**O**) Percentages of c-Fos^+ cells in the PFC of the HC, context exposure (CTX), CFC with eYFP, and CFC with eArchT groups. (**P**) Virus-mediated engram cell labeling with ChR2. (**Q**) Coronal section of PFC with ChR2-mCherry (red). (**R** and **T**) Experimental schedules. (**S** and **U**) Averaged freezing for blue light–off and blue light–on epochs. (**V**) Retrograde transsynaptic labeling with activity-dependent cell labeling. (**W**) Sagittal section of MEC with rabies virus–specific mCherry (red). (**X**) Distribution of 212 mCherry$^+$ cells in the MEC. *$P < 0.05$; unpaired t test compared with eYFP [(F), (G), (K), and (L)], one-way analysis of variance (ANOVA) with Tukey-Kramer test (O), or paired t test [(S) and (U)]. Graphs show means ± SEM (in the bar graphs, circles and red lines represent individual animals). Lightning bolt, footshock; polyA, polyadenylation signal; DAPI, 4′,6-diamidino-2-phenylindole; "A", context A (conditioned context); "B", context B (unconditioned context); OFF-Dox, off doxycycline; ON-Dox, on doxycycline.

PFC engram cells by green light during retrieval did not affect recent memory (day 2); however, at the remote time point (day 12), memory retrieval was disrupted compared with the green light–off condition (Fig. 2F).

To further investigate the characteristics of PFC engram cells, we monitored transient calcium (Ca^{2+}) events in PFC cells in vivo. WT mice were injected with AAV_5-human synapsin1 (Syn): GCaMP6f in the PFC and implanted with a micro–gradient-index (GRIN) lens targeting the PFC (Fig. 2, G to I, and fig. S8) (*22*, *27*). On day 1, mice were first exposed to context B, followed by CFC in context A. Mice were then reexposed to both contexts in the same order on days 2 and 15 (Fig. 2J). The averaged frequency of Ca^{2+} events in PFC cells did not significantly change in either a time- or context-dependent manner (fig. S9B). However, a small but significant difference was revealed in the cumulative distribution curves of a rate difference index (assessing context selectivity; see the methods) between day 1 conditioning and day 15 recall and between day 2 recall and day 15 recall (fig. S9C). PFC cells did not appear to discriminate between the two contexts on day 1 before footshock presentation (Fig. 2, K and L). However, after footshock presentation, about 11% of cells showed a significant increase in Ca^{2+} transients [shock-responding (SR) cells] (Fig. 2, K and L). The remaining ~89% of PFC cells did not respond to the shocks [shock-nonresponding (SNR) cells]. The SR cells were less active than the SNR cells during exposure to contexts B and A on day 1 before footshock presentation (Fig. 2, L to N, and fig. S9D). During recall, the transient Ca^{2+} activity of SR cells in context A was significantly higher compared with that in context B on day 15, but not on days 1 or 2, whereas the frequency of Ca^{2+} transient events in SNR cells remained constant, irrespective of context (Fig. 2, M and N). This produced a significant rate difference index of Ca^{2+} activity for context A between the SR and SNR cells on day 15 but not on day 1 (excluding the shock delivery period) or day 2 (Fig. 2O). These results,

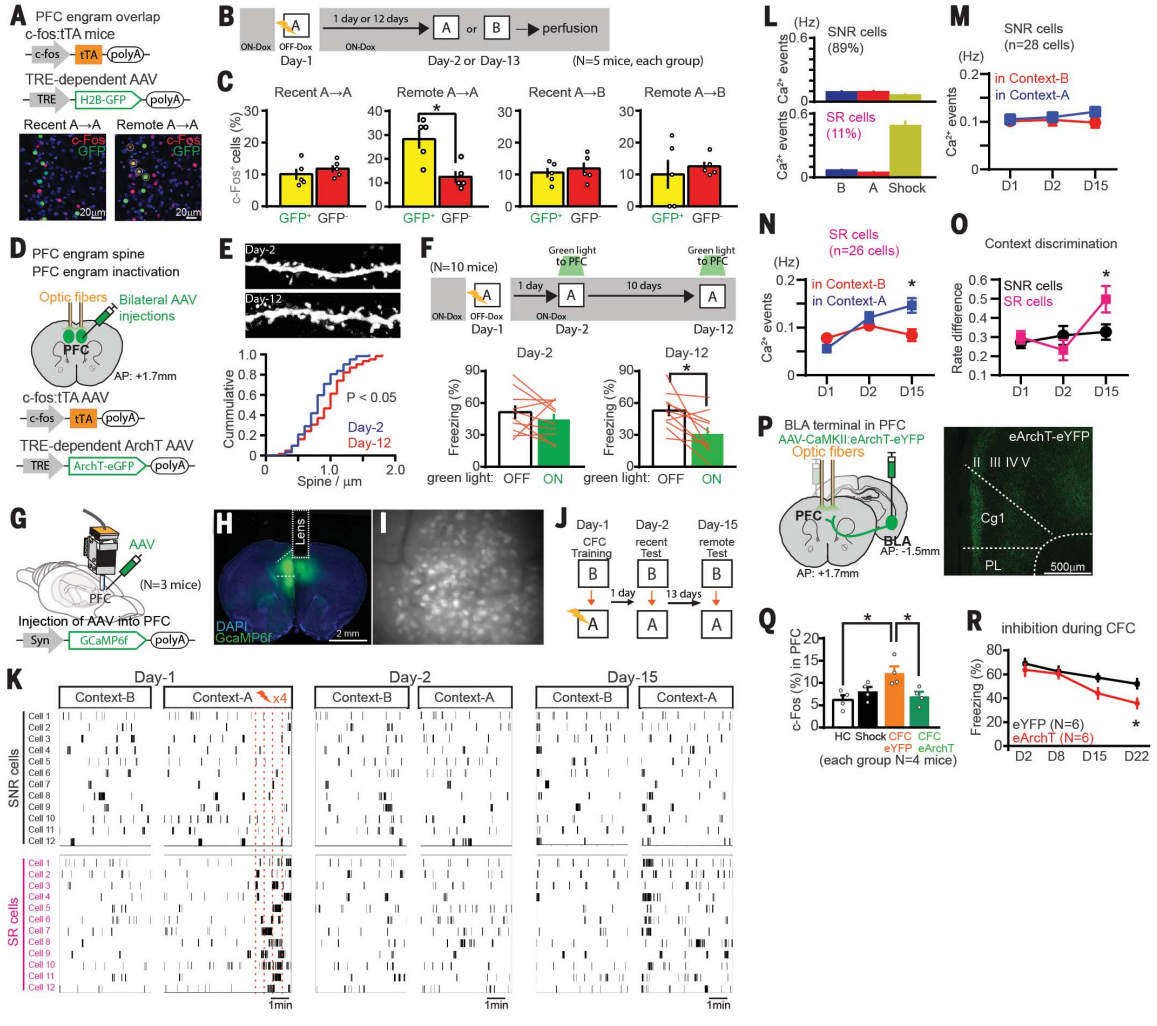

Fig. 2. PFC engram cells mature with time. (**A**) PFC engram cell labeling with H2B-GFP (top) and coronal sections of PFC with H2B-GFP (green) and anti–c-Fos (red) (bottom). Circled cells are double-positive. (**B**) Experimental schedule. (**C**) Percentages of c-Fos$^+$ cells in H2B-GFP$^+$ and H2B-GFP$^-$ cells in PFC. (**D**) PFC engram cell labeling with ArchT. (**E**) Dendritic spines from PFC engram cells (top) and cumulative probability of the spine density of PFC engrams (bottom). (**F**) Experimental schedule (top) and averaged freezing for green light–off and green light–on epochs during recall testing (bottom). (**G** and **H**) Viral injections and GRIN lens implantation. (**I**) Stacked image acquired through the microendoscope over 10 min of imaging in the PFC. (**J**) Experimental schedule. (**K**) Raster plots of Ca^{2+} events (black bars) in shock-nonresponding (SNR) and shock-responding (SR) cells in the PFC (showing 12 example cells). (**L** to **N**) Averaged Ca^{2+} event frequency for SNR and SR cells on days 1, 2, and day 15. (**O**) Averaged rate difference index of Ca^{2+} activity. (**P**) Viral injections and optic fiber implantations (left) and coronal sections of PFC visualizing BLA axons (green) (right). Cg1, cingulate cortex 1 (rACC). (**Q**) Percentages of c-Fos$^+$ cells in the PFC of the HC, shock only, CFC with eYFP, and CFC with eArchT groups. (**R**) Time courses of freezing during recall tests. *$P < 0.05$; unpaired t test [(C), (O), and (R)], Kolmogorov-Smirnov (KS) test (E), paired t test [(F), (M), and (N)], or one-way ANOVA with Tukey-Kramer test (Q). Graphs show means ± SEM.

combined with c-Fos activation data (Fig. 1, M to O), suggest that the SR cells may be the PFC memory engram cells, given that the generation of the PFC engram cells requires both context exposure and footshocks.

Our calcium imaging data suggest that footshock stimulus input into the PFC is crucial for the generation of PFC engram cells. Because the BLA integrates footshock information arriving from the thalamus (*28*) and projects to the PFC (figs. S5I and S10), we optogenetically inhibited the pathway from the BLA to the PFC during CFC (Fig. 2P). Optogenetic inhibition of BLA terminals in the PFC during CFC disrupted the generation of PFC engram cells (Fig. 2Q). The terminal inhibition during CFC also inhibited remote memory formation (Fig. 2R).

To test whether the HPC engram cells play a crucial role in the functional maturation of PFC engram cells during the systems consolidation process, we bilaterally targeted injection of AAV_9-TRE:tetanus toxin light chain (TeTX) or AAV_9-TRE:eYFP (as a control) to the hippocampal dentate gyrus (DG) of c-fos:tTA transgenic mice (Fig. 3A). When the mice were subjected to CFC, DG engram cells were labeled with TeTX. DG engram cell labeling with TeTX caused a robust inhibition of DG engram cell output, as revealed by greatly reduced immunoreactivity of vesicle-associated membrane protein 2 (VAMP2)—which is essential for activity-dependent neurotransmitter release from presynaptic terminals (*13*)—within the stratum lucidum in hippocampal CA3 in mice that were off doxycycline, compared with that in mice that were on doxycycline (Fig. 3, B and C). In TeTX-expressing mice, optogenetic activation of DG engram cells with ChR2 failed to produce the increase in CA3 c-Fos$^+$ cells that was observed in eYFP control mice relative to home-cage controls (Fig. 3D). TeTX expression in HPC engram cells inhibited the reactivation of PFC engram cells, compared with that in the eYFP control group, during exposure to context A 12 days after CFC (Fig. 3, E and F). TeTX expression also blocked the increase in the dendritic spine density of PFC engram cells that was observed in the eYFP group (Fig. 3G). In vivo calcium imaging revealed that TeTX expression in HPC engram cells after CFC blocked the increase in the context discrimination index in SR cells in the PFC (Fig. 3H and fig. S11).

To investigate the postconsolidation fate of HPC engram cells, we crossed c-fos:tTA transgenic mice with TRE:H2B–GFP transgenic mice (*29*), subjected them to CFC, then reexposed them to context A (the conditioned context) or context B (an unconditioned context) on day 2

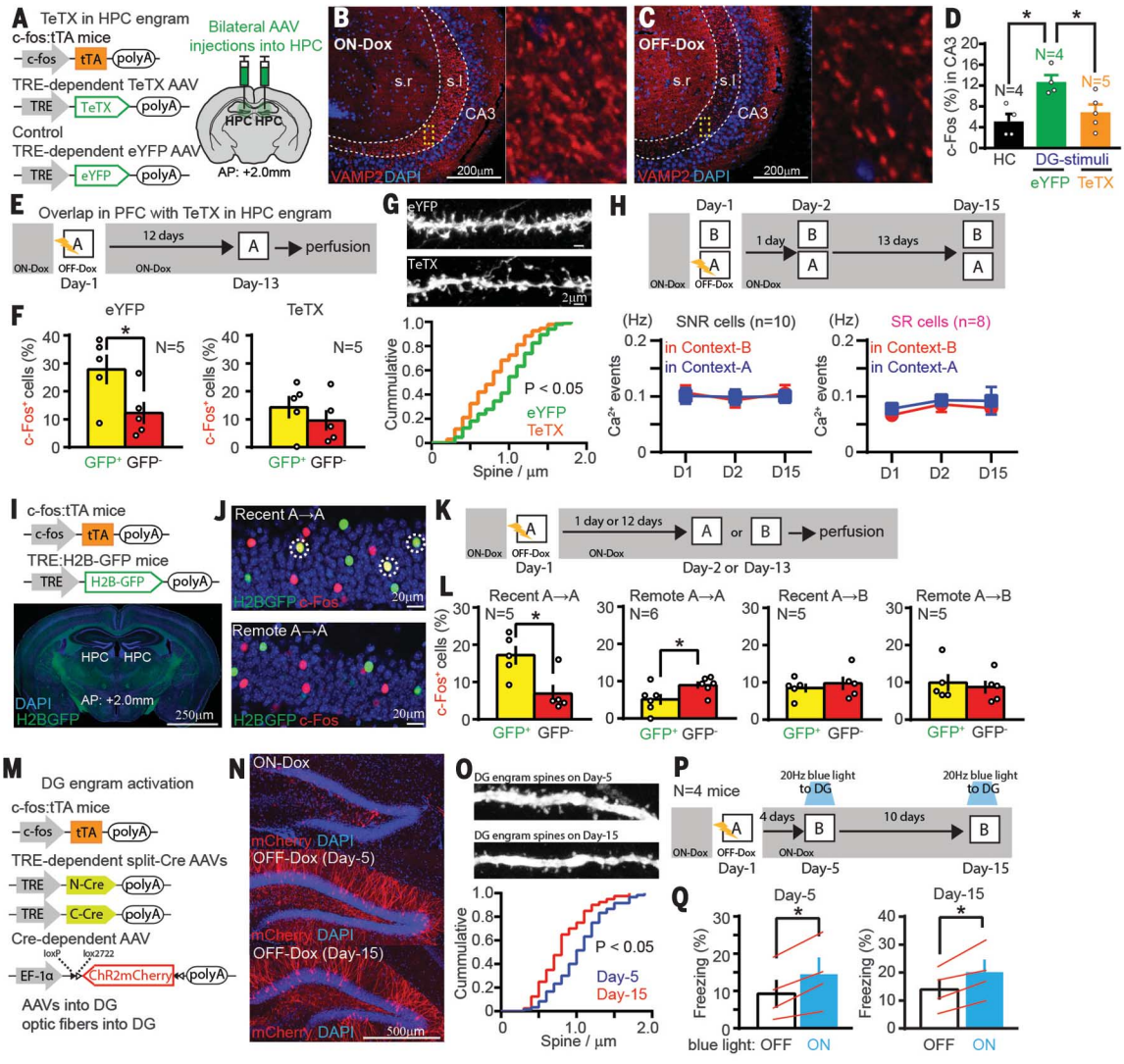

Fig. 3. HPC engram cells support the maturation of PFC engram cells and become silent with time. (**A**) DG engram cell labeling with TeTX. (**B** and **C**) Sagittal sections of HPC with anti-VAMP2 (red). The yellow box indicates the area of magnification (right). s.r., stratum radiatum; s.l., stratum lucidum. (**D**) Percentages of c-Fos$^+$ cells in hippocampal CA3 of the HC, blue light–on mice with eYFP, and blue light–on mice with TeTX. (**E**) Experimental schedule. (**F**) Percentages of c-Fos$^+$ cells in H2B-GFP$^+$ and H2B-GFP$^-$ cells in the PFC of eYFP- and TeTX-expressing mice. (**G**) Dendritic spines from PFC engrams (top) and cumulative probability of the spine density of PFC engrams in eYFP- and TeTX-expressing mice (bottom). (**H**) Experimental schedule (top) and averaged Ca^{2+} event frequency of SNR and SR cells under the TeTX-expressing condition (bottom). (**I**) Transgenic strategy of DG engram cell labeling with H2B-GFP (top) and coronal section of the brain (bottom). (**J**) Coronal sections of DG with H2B-GFP (green) and anti–c-Fos (red). Circled cells are double-positive. (**K** and **P**) Experimental schedules. (**L**) Percentages of c-Fos$^+$ cells in H2B-GFP$^+$ and H2B-GFP$^-$ cells in the DG. (**M**) Long-term DG engram cell labeling with ChR2. (**N**) Coronal sections of DG with ChR2-mCherry (red). (**O**) Dendritic spines from DG engrams (top) and cumulative probability of the spine density of DG engrams (bottom). (**Q**) Averaged freezing for blue light–off and blue light–on epochs. *P < 0.05; one-way ANOVA with Tukey-Kramer test (D), unpaired t test [(F) and (L)], KS test [(G) and (O)], or paired t test [(H) and (Q)]. Graphs show means ± SEM.

or 13 (Fig. 3, I to K). Compared with the non-engram cells, DG engram cells were preferentially reactivated in context A on day 2, but not on day 13 (Fig. 3L). No difference was observed in the activation of DG engram and non-engram cells by context B (Fig. 3L). We were unable to maintain labeled DG engram cells with ChR2 beyond 12 days with injection of AAV_9-TRE:ChR2-mCherry. To extend this technical limit, we targeted injections of $AAV_{1,5,8,9}$-TRE:CCre, $AAV_{1,5,8,9}$-TRE:NCre, and AAV_5-elongation factor 1a (EF1a):ChR2-mCherry to the DG of c-fos:tTA transgenic mice (Fig. 3M). We could thus extend viable labeling by a few days (Fig. 3N). The spine density of DG engram cells on day 15 was significantly reduced compared with that on day 5 (Fig. 3O and fig. S12). On both days 5 and 15, optogenetic activation of DG engram cells induced freezing behavior (Fig. 3, P and Q).

Last, we investigated the role of MEC-Va projections into the BLA in recent and remote memory (Fig. 4A and fig. S2A). Inhibition of MEC-Va terminals in the BLA during CFC disrupted contextual fear memory formation. Retrieval was impaired at all time points tested (Fig. 4B). When terminal inhibition was restricted to retrieval, recent memory tested on days 2 and 8 was impaired, but remote memory retrieval on days 15 and 22 was unaffected (Fig. 3C). In contrast, inhibition of PFC engram cell terminals in the BLA did not impair memory retrieval on day 2 but did impair memory retrieval on day 12 (Fig. 4, D and E). To investigate whether the BLA fear memory engram cells formed on day 1 are maintained and used for PFC engram-dependent remote memory recall, we subjected the double transgenic mice (Fig. 4, F and I) to CFC and reexposed them to context A at recent or remote time points (Fig. 4G). BLA engram cells were reactivated equally well by context A at recent and remote time points (Fig. 4H). Similarly, BLA cells activated by recent recall were reactivated equally well by reexposure to context A at recent and remote time points (Fig. 4, J and K).

In this study, we found that PFC memory engram cells for CFC were rapidly formed during day 1 training through inputs from both the MEC-Va and the BLA, but they were not retrievable with natural recall cues. The immature PFC engram cells functionally, structurally,

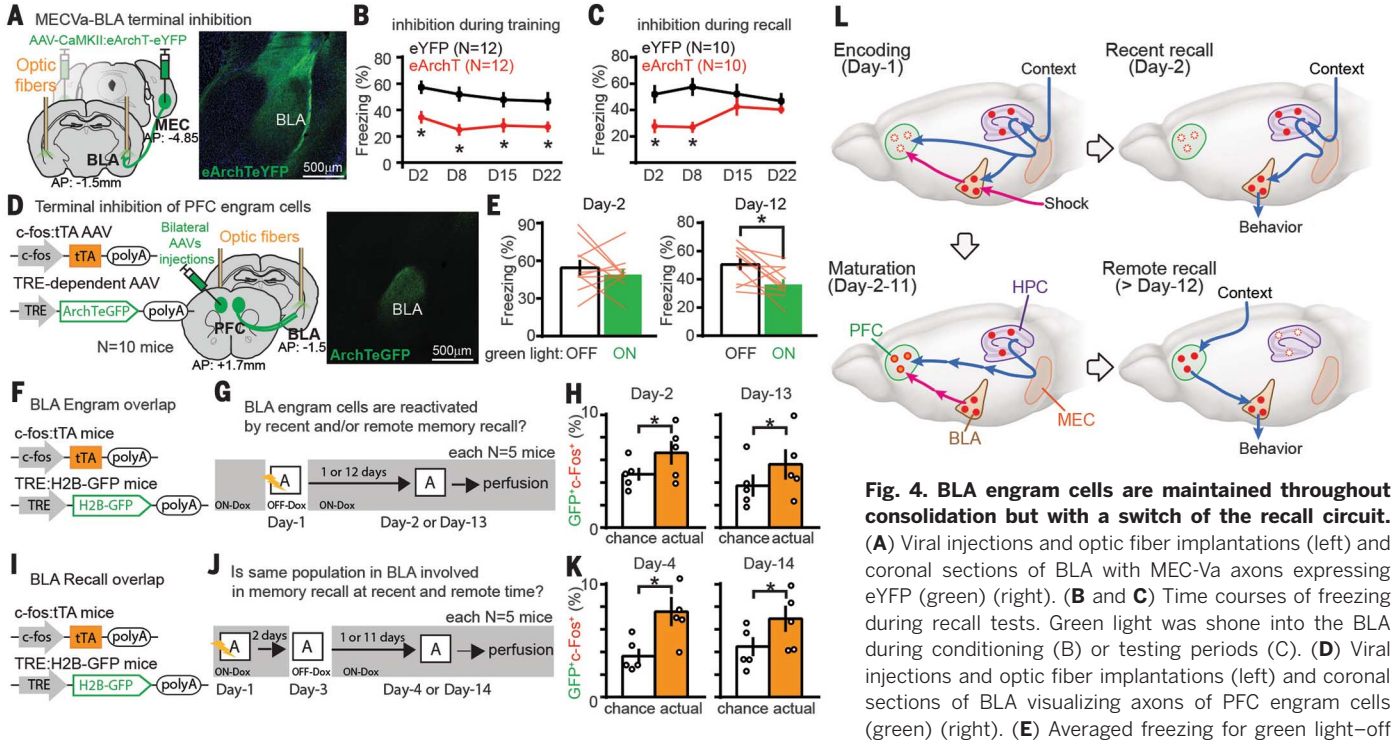

Fig. 4. BLA engram cells are maintained throughout consolidation but with a switch of the recall circuit. (**A**) Viral injections and optic fiber implantations (left) and coronal sections of BLA with MEC-Va axons expressing eYFP (green) (right). (**B** and **C**) Time courses of freezing during recall tests. Green light was shone into the BLA during conditioning (B) or testing periods (C). (**D**) Viral injections and optic fiber implantations (left) and coronal sections of BLA visualizing axons of PFC engram cells (green) (right). (**E**) Averaged freezing for green light–off and green light–on epochs during recall testing. (**F** and **I**) BLA engram cell labeling with H2B-GFP. (**G** and **J**) Experimental schedules. (**H** and **K**) Percentages of double-labeling with c-Fos and H2B-GFP in the BLA compared with the calculated chance percentages. (**L**) A new model for systems consolidation of memory. *$P < 0.05$; unpaired t test [(B), (C), (H), and (K)] or paired t test (E). Graphs show means ± SEM.

and physiologically matured during the subsequent few weeks, and this process required inputs from HPC engram cells, presumably through the MEC-Va. In contrast to their formation on day 1, retrieval of the PFC engram at a remote time did not require MEC-Va input. HPC engram cells that formed during training became silent with time; they were not retrieved on day 14 by natural recall cues but were still reactivatable optogenetically for recall. However, fear memory BLA engrams that formed during training were functionally maintained, even after the consolidation-mediated switch in recall circuits (Fig. 4L).

Our model (Fig. 4L) introduces the concept that the prefrontal memory engram is already generated, albeit in an immature form, on day 1 of training through inputs from both the HPC-EC network and the BLA (Fig. 1). The standard model (*1*, *2*, *4*, *6*, *7*, *11*) hypothesizes that remote memory is formed in the cortex by a slow transfer of hippocampal memory. In contrast, in our study, the role of the hippocampus in cortical memory is in the rapid generation of immature engram cells in the PFC during training and in the subsequent functional maturation of these preexisting engram cells (Fig. 2). The immature PFC engram may correspond to the cortical "tagging" suggested in an earlier study (*14*). In a previous study, the BLA was found to be crucial for both recent and remote fear memory expression (*30*). Our results demonstrate an overlapping set of BLA engram cells for both recent and remote fear memory retrieval, which were quickly formed during training (Fig. 4). However, the source of input into the BLA engrams for retrieval shifts from the MEC-Va at recent time points to the PFC engram at remote time points (Fig. 4L). The route through which contextual stimuli activate the mature PFC engram is unknown. Most likely, the information processed in a variety of sensory cortices reaches the PFC via the thalamus (*31*). Supporting this idea, PFC engram cells receive monosynaptic input from both the medial-dorsal and anteromedial thalamus (fig. S5).

Our finding of the lasting hippocampal engrams (Fig. 3Q) is consistent with multiple trace theory (*5*, *11*). However, at the postconsolidation stage, the hippocampal engrams were not activatable by natural recall cues, but rather by optogenetic stimulation. A similar state of hippocampal engrams has previously been observed in anisomycin-induced amnesia (*24*) and mouse models of early Alzheimer's disease (*26*), and the early (day 2) PFC engram cells showed a similar property (Figs. 1S and 2C). Although we did not determine how long after encoding this "silent state" of the hippocampal engram lasts, we speculate that the hippocampal engram eventually loses the original memory information (*29*, *32*, *33*). Alternatively, the silent engram cells may still participate in the successful remote recall of discrete episodic details (*5*, *11*).

As in previous studies (*18*, *20*, *29*), we observed that training resulted in widespread neuronal activation in the neocortex, including the ACC and RSC. However, whereas the activation of PFC neurons is crucial for formation of remote memory, MEC-Va input into the cACC or RSC is dispensable for this process. For remote memory, the PFC may thus have a distinctive role in integrating multiple sensory information stored in various cortical areas (*11*). Last, our data show that the remote memory expressed by the PFC engram is conditioned-context specific, suggesting that it is episodic-like.

REFERENCES AND NOTES

1. D. Marr, *Philos. Trans. R. Soc. London B Biol. Sci.* **262**, 23–81 (1971).
2. L. R. Squire, *Science* **232**, 1612–1619 (1986).
3. J. J. Kim, M. S. Fanselow, *Science* **256**, 675–677 (1992).
4. J. L. McClelland, B. L. McNaughton, R. C. O'Reilly, *Psychol. Rev.* **102**, 419–457 (1995).
5. L. Nadel, M. Moscovitch, *Curr. Opin. Neurobiol.* **7**, 217–227 (1997).
6. D. Tse *et al.*, *Science* **316**, 76–82 (2007).
7. J. L. McClelland, *J. Exp. Psychol. Gen.* **142**, 1190–1210 (2013).
8. G. Buzsáki, *Cereb. Cortex* **6**, 81–92 (1996).
9. A. G. Siapas, M. A. Wilson, *Neuron* **21**, 1123–1128 (1998).
10. B. J. Wiltgen, R. A. Brown, L. E. Talton, A. J. Silva, *Neuron* **44**, 101–108 (2004).
11. P. W. Frankland, B. Bontempi, *Nat. Rev. Neurosci.* **6**, 119–130 (2005).
12. A. R. Preston, H. Eichenbaum, *Curr. Biol.* **23**, R764–R773 (2013).
13. T. Nakashiba, D. L. Buhl, T. J. McHugh, S. Tonegawa, *Neuron* **62**, 781–787 (2009).
14. E. Lesburguères *et al.*, *Science* **331**, 924–928 (2011).
15. M. Zelikowsky, S. Bissiere, M. S. Fanselow, *J. Neurosci.* **32**, 3393–3397 (2012).
16. L. G. Reijmers, B. L. Perkins, N. Matsuo, M. Mayford, *Science* **317**, 1230–1233 (2007).
17. X. Liu *et al.*, *Nature* **484**, 381–385 (2012).

18. S. Tonegawa, X. Liu, S. Ramirez, R. Redondo, *Neuron* **87**, 918–931 (2015).
19. T. Kitamura *et al.*, *Science* **343**, 896–901 (2014).
20. L. Ye *et al.*, *Cell* **165**, 1776–1788 (2016).
21. K. Deisseroth, *Nat. Neurosci.* **18**, 1213–1225 (2015).
22. Y. Ziv *et al.*, *Nat. Neurosci.* **16**, 264–266 (2013).
23. G. Sürmeli *et al.*, *Neuron* **88**, 1040–1053 (2015).
24. T. J. Ryan, D. S. Roy, M. Pignatelli, A. Arons, S. Tonegawa, *Science* **348**, 1007–1013 (2015).
25. A. Hayashi-Takagi *et al.*, *Nature* **525**, 333–338 (2015).
26. D. S. Roy *et al.*, *Nature* **531**, 508–512 (2016).
27. T. Kitamura *et al.*, *Neuron* **87**, 1317–1331 (2015).
28. B. A. Pellman, J. J. Kim, *Trends Neurosci.* **39**, 420–431 (2016).
29. K. K. Tayler, K. Z. Tanaka, L. G. Reijmers, B. J. Wiltgen, *Curr. Biol.* **23**, 99–106 (2013).
30. S. Maren, G. Aharonov, M. S. Fanselow, *Behav. Neurosci.* **110**, 718–726 (1996).
31. F. H. Do-Monte, K. Quiñones-Laracuente, G. J. Quirk, *Nature* **519**, 460–463 (2015).
32. C. A. Denny *et al.*, *Neuron* **83**, 189–201 (2014).
33. T. Kitamura *et al.*, *Cell* **139**, 814–827 (2009).

ACKNOWLEDGMENTS

We thank F. Bushard, J. Martin, T. Ryan, J. Yamamoto, C. Sun, W. Yu, S. Huang, M. Ragion, A. Arons, X. Zhou, C. Ragion, A. Moffa, L. Brenner, A. Hamalian, and D. King for help with experiments and preparing the manuscript; all members of the Tonegawa laboratory for their support; I. Wickersham for providing rabies virus; and Y. Shima and S. B. Nelson for providing TRE3G split Cre AAV. All data necessary to understand and assess the conclusions of this research are available in the supplementary materials. This work was supported by the RIKEN Brain Science Institute, the Howard Hughes Medical Institute, and the JPB Foundation (to S.T.). AAV_9–c-fos: tTA, AAV_9-TRE:ChR2mCherry, AAV_9-TRE:ArchTeGFP, AAV_9-TRE: TeTX, and AAV_9-TRE:eYFP were developed at the Massachusetts Institute of Technology by the group of S.T.; virus plasmids are available through a material transfer agreement.

SUPPLEMENTARY MATERIALS

www.sciencemag.org/content/356/6333/73/suppl/DC1
Materials and Methods
Supplementary Text
Figs. S1 to S12
References (*34*–*51*)

28 December 2016; accepted 14 March 2017
10.1126/science.aam6808

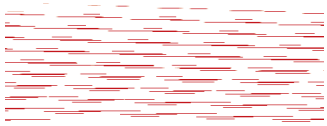

Engrams and circuits crucial for systems consolidation of a memory

Takashi Kitamura, Sachie K. Ogawa, Dheeraj S. Roy, Teruhiro Okuyama, Mark D. Morrissey, Lillian M. Smith, Roger L. Redondo and Susumu Tonegawa (April 6, 2017)

Science **356** (6333), 73-78. [doi: 10.1126/science.aam6808]

Editor's Summary

The network of memory consolidation

Memories are thought to be formed in the hippocampus and later moved to the neocortex for long-term storage. However, little is known about the mechanisms that underlie the formation and maturation of neocortical memories and their interaction with the hippocampal network. Kitamura *et al.* discovered that at the onset of learning, neurons for contextual fear memory are quickly produced in the prefrontal cortex. This process depends on the activity of afferents from both the hippocampus and the amygdala. Over time, the prefrontal neurons consolidate their role in memory expression. In contrast, the hippocampal neurons slowly lose this function.

Science, this issue p. 73

www.sciencemag.org/content/356/6333/73/suppl/DC1

Supplementary Materials for

Engrams and circuits crucial for systems consolidation of a memory

Takashi Kitamura,* Sachie K. Ogawa,* Dheeraj S. Roy,* Teruhiro Okuyama, Mark D. Morrissey, Lillian M. Smith, Roger L. Redondo, Susumu Tonegawa†

*These authors contributed equally to this work.
†Corresponding author. Email: tonegawa@mit.edu

Published 7 April 2017, *Science* **356**, 73 (2017)
DOI: 10.1126/science.aam6808

This PDF file includes:

Materials and Methods

Subjects

All procedures relating to mouse care and treatment conformed to institutional and NIH guidelines. Animals were individually housed in a 12 hour (7am-7pm) light/dark cycle, with food and water ad libitum. We used 15-25 weeks-old wild-type male C57BL/6J mice (WT: Jackson Laboratory), c-fos:tTA transgenic mice (Jackson Laboratory; strain B6.Cg-Tg(Fos-tTA,Fos-EGFP*)1Mmay/J; stock number 018306) (*16*) and TRE:H2B-GFP transgenic mice (Jackson Laboratory: strain Tg(tetO-HIST1H2BJ/GFP)47Efu/J; stock number 005104) (*29*, *34*).

Preparation of Adeno-Associated Viruses

The pAAV-TRE:ChR2-mCherry, pAAV- TRE:ArchT-eGFP, pAAV-TRE:HTG plasmids (Addgene plasmid # 27437) and pAAV-c-fos:tTA were constructed as previously reported (*26, 35-38*). The pAAV-TRE:TeTX was constructed by replacing the ChR2-eYFP fusion gene in the pAAV-TRE:ChR2-eYFP plasmid from Liu et al. (*17*) with a gene of TeTX-LC from pGEMTEZ-TeTXLC (a gift from Richard Axel & Joseph Gogos & C. Ron Yu (Addgene plasmid # 32640) (*39*). These plasmids were used to generate by the Gene Therapy Center and Vector Core at the University of Massachusetts Medical School or ViGENE Biosciences. Viral titrations were 8.0*10^12 genome copy per ml for AAV_9-TRE:ChR2-mCherry, 1.0*10^13 genome copy per ml for AAV_9-TRE:ArchT-eGFP, 1.4*10^13 genome copy per ml for AAV_5-TRE:HTG, 1.5*10^13 genome copy per ml for AAV_9-c-fos:tTA and 3.7*10^14 genome copy per ml for AAV_9-TRE:TeTX. For the long-term labeling of DG engram cells, we employed split-Cre AAV constructs, in which the Cre coding sequence is divided into N-terminus (NCre) and C-terminus (CCre) parts and their dimerization via a leucine zipper re-forms the functional enzyme (*40*). TRE3G split Cre AAV (TRE3G:NCre and TRE3G:CCre) did not have detectable leak expression in 293T cells or in the brain (*41*). $AAV_{1,5,8,9}$-TRE3G:NCre (5.7*10^13 genome copy/ml) and $AAV_{1,5,8,9}$-TRE3G:CCre (1.6*10^13 genome copy/ml) were generated with the a cocktail of 4 serotypes (2/1, 2/5, 2/8, 2/9) by Yasuyuki Shima and Sacha B Nelson (Brandeis University) in house (*41*). The AAV_5-CaMKIIα:eYFP (5.2*10^12 genome copy/ml), AAV_5-CaMKIIα:eArchT-eYFP (2.5*10^12 genome copy/ml), AAV_8-CaMKIIα:eYFP (3.5*10^12 genome copy/ml) and AAV_8-CaMKIIα:eArchT-eYFP (2.7*10^12 genome copy/ml) and AAV_9-

CaMKIIα:eArchT-eYFP (2.0*10^13 genome copy/ml) were generated by and acquired from the University of North Carolina at Chapel Hill (UNC) Vector Core. The AAV_5-Syn:GCaMP6f (1.5*10^13 genome copy/ml) and AAV_5-EF1α:DIO-ChR2-mCherry (2.0*10^13 genome copy/ml) was generated by and acquired from the University of Pennsylvania Vector Core.

Preparation of Rabies Virus

Deletion-mutant rabies virus was produced by replacing the eGFP gene in cSPBN-4GFP with the gene encoding mCherry. Packaging with the ASLV-A envelope protein was made as previously described (*42, 43*).

Stereotactic Injection and Fiber Optic Implants

Stereotactic viral injections, microendoscope implantations, and optic fiber implantations were all performed in accordance with MIT's CAC guidelines. Mice were anaesthetized using 500 mg/kg avertin. Viruses were injected using a glass micropipette attached to a 10 μl Hamilton microsyringe through a microelectrode holder filled with mineral oil. A microsyringe pump and its controller were used to control the speed of the injection. The needle was slowly lowered to the target site and remained for 10 minutes after the injection. For the terminal inhibition of MEC-Va projection at PFC, cACC (caudal part of ACC), RSC and BLA, bilateral viral delivery into MEC of WT male mice was aimed at these coordinates relative to Bregma: AP: -4.85 mm, ML, ±3.45 mm, DV, -3.30 mm. Mice were bilaterally injected with 200 nl of AAV_8-CaMKIIα:eArchT-eYFP or AAV_8-CaMKIIα:eYFP as control group, and were bilaterally implanted with optical fibers into the PFC (AP: +1.7 mm, ML, ±0.35 mm, DV, -1.6 mm), cACC (AP: ±0.0 mm, ML, ±0.35 mm, DV, -1.2 mm, posterior part of ACC), RSC (AP: -1.94 mm, ML, ±0.35 mm, DV, -0.75 mm) or BLA (AP −1.5 mm, ML +3.3 mm, DV −4.3 mm). For the terminal inhibition of BLA cells at PFC, bilateral viral delivery into BLA of WT male mice was aimed at these coordinates relative to Bregma: AP: -1.5 mm, ML, ±3.3 mm, DV, -4.68 mm. Mice were bilaterally injected with 150 nl of AAV_9-CaMKIIα:eArchT-eYFP or AAV_9-CaMKIIα:eYFP as control group, and were bilaterally implanted with optical fiber into the PFC (AP: +1.7 mm, ML, ±0.35 mm, DV, -1.6 mm). For the cell body activation/inhibition of PFC engram cells, c-fos:tTA mice were bilaterally injected with 150 nl of AAV_9-TRE:ArchT-eGFP or AAV_9-TRE:ChR2-mCherry into the PFC (AP: +1.7 mm, ML, ±0.35 mm, DV, -1.7 mm), and were

bilaterally implanted with optical fiber into the PFC (AP: +1.7 mm, ML, ±0.35 mm, DV, -1.6 mm) under the ON-Dox condition. For the cell body activation of DG engram cells, c-fos:tTA mice were bilaterally injected with 200 nl of AAV_9-TRE:ChR2-mCherry into the DG (AP: -2.0 mm, ML, ±1.3 mm, DV, -2.05 mm), and were bilaterally implanted with optical fiber into the DG (AP: -2.0 mm, ML, ±1.3 mm, DV, -1.5 mm) under the ON-Dox condition. The top part of an Eppendorf tube was inserted to protect the implant and the incision was closed with sutures(*17*)[10]. 100 nl of CTB-Alexa555 (0.5 % wt/vol) was unilaterally injected into PFC (AP: +1.7 mm, ML, +0.35 mm, DV, -1.7 mm), caudal ACC (cACC, AP: ±0.0 mm, ML, +0.35 mm, DV, -1.2 mm), RSC (AP: -1.94 mm, ML, +0.35 mm, DV, -0.75 mm) or BLA (AP −1.5 mm, ML +3.3 mm, DV −4.68 mm). Five to seven days after the CTB injection. Mice were perfused for brain sampling. For the GCaMP6f activity monitoring from the PFC, bilateral viral delivery into the PFC of the WT male mice was aimed at these coordinates relative to Bregma: AP: -1.78 mm, ML, ±1.3 mm, DV, -1.7 mm. WT mice were bilaterally injected with 150 nl of AAV2/5-Syn:GCaMP6f. One month after AAV injection, we implanted a microendoscope into the right side of PFC (AP: -1.78 mm, ML, +0.35 mm, DV, -1.6 mm) of the WT mice. One month after implantation of the microendoscope, the baseplate for a miniaturized microscope camera (*22*, *27*) was attached above the implanted microendoscope in the mice. After the baseplate surgery, animals were habituated to the attachment of the microscope camera for two weeks.

Histology

Mice were transcardially perfused with 4 % paraformaldehyde (PFA) in phosphate buffered saline (PBS). Brains were post-fixed with the same solution for 24 hours, and then sectioned using a vibratome by sagittal sections or coronal sections depends on purpose of experiments. For immunohistochemistory, sliced tissue sections were incubated in 0.3 % Triton-X PBS with 5 % normal goat serum (NGS) for 1 hour. Primary antibodies were then added to a 5 % NGS 0.3 % triton-X in PBS solution and incubated overnight at 4°C. Primary antibodies: chicken anti-GFP antibody (Thermo Fisher Scientific, A-10262, 1:1000), rabbit anti-PCP4 antibody (Sigma, HPA005792-100UL, 1:200), mouse anti-NeuN antibody (Millipore, MAB377, 1:1000), rabbit anti-c-Fos antibody (Santa Cruz Biotechnology, SC-52, 1/500), rabbit anti-RFP antibody (Rockland, 600-401-379, 1/1000), and rabbit anti-VAMP2 antibody (Synaptic Systems, 104 202, 1/250). After rinsing with PBS 3 times for 15 min each, sliced tissue sections were subsequently

incubated with AlexaFluor405, AlexaFluor488, AlexaFluor546, or AlexaFluor633 conjugated secondary antibodies (Thermo Fisher Scientific, 1:250). Sliced tissue sections were then washed in PBS 3 times for 15 min and mounted in VECTASHIELD antifade mounting medium for Fluorescence on glass slides. Some sections were stained by DAPI or Nissl (1:500). Fluorescence images were taken by confocal microscopy using 10X, 20X, 40X, 63X objectives and by fluorescent microscopy using 10Xand 20X objectives. Z-projected confocal images were generated by Zenblack.

Contextual Fear Conditioning and Recall Testing

Fear conditioning was performed on male mice aged between 15 and 25 weeks, in the animal facility during the light cycle with minor modifications to the method described previously (*19, 27*). Before fear conditioning, all animals were habituated to human experimenters for 3 days. For contextual fear conditioning, we used two different contexts (Context-A and Context-B). Context-A was a chamber (29 cm (W) x 23 cm (D) x 20 cm (H)) with distinct visual cues and a grid floor which consisted of 36 stainless steel rods (Context-A). Context-B was a chamber (29 cm (W) x 23 cm (D) x 20 cm (H)) with different visual cues, compared to Context-A, and has a white plastic floor (Context-B). These chambers were cleaned with 70% ethanol prior to the introduction of each individual mouse. When we examined the terminal inhibition during conditioning (fig, S1E), on Day-1, the optical fiber implants was bilaterally connected to a 561 nm laser controlled by a function generator and green light stimulation (15 mW, each hemisphere) was illuminated during the entire training period (300 s). Subject mice were kept in the conditioning chamber in Context-A for total 300 s. Foot-shock (2 s, 0.75mA) was delivered at 120 s, 180 s and 240 s. Mice remained in the conditioning chamber for a total of 300 s. On Day-2, Day-8, Day-15, Day-22, mice were placed into Context-A (or Context-B) and allowed to explore for 180 s to monitor their freezing behavior. When we examined the terminal inhibition during recall testing (fig, S1F), on Day-1, subject mice were kept in the conditioning chamber in Context-A for total 300 s. Foot-shock (2 s, 0.75mA) was delivered at 120 s, 180 s and 240 s. Mice remained in the conditioning chamber for a total of 300 s. On Day-2, Day-8, Day-15 and Day-22, the optical fibe implants was bilaterally connected to a 561 nm laser controlled by a function generator and green light stimulation (15 mW, each hemisphere) was illuminated during the entire testing period (180 s) in Context-A (or Context-B).

Activity-Dependent Cell Labeling

For activity-dependent cell labeling, we employed c-fos:tTA transgenic mice combined with AAV-TRE system or TRE transgenic mice (*16*) (*17, 29, 37, 38*), a) AAV_9-TRE:ChR2-mCherry, AAV_9-TRE:ArchT-eGFP or AAV_5-TRE:HTG injection into c-fos:tTA mice, and b) c-fos:tTA mice crossed with TRE:H2B-GFP transgenic mice. These mice were maintained under the food condition containing 40 mg/kg Dox from their birth. Mice were single housed post-surgery and throughout the rest of the experiments. Before labeling cells, all animals were habituated to human experimenters for 3 days. In order to open a window of activity-dependent labeling for CFC in Context-A, the mice were then taken off Dox for 24 hours. Animals were exposed to Context-A for 300 s for CFC, and DOX diets were resumed immediately after CFC. When we did not open a window for activity-dependent labeling during CFC, there was no cell labeling in PFC, DG, nor BLA (Fig. 1Q, fig. S6). Moreover, there was no reduction of number of H2BGFP positive cells in PFC, DG, and BLA through the 12 days after CFC. In the DG engram cells labeling with ChR2, we have a slight reduction of the expression of ChR2 in DG engram cells. So, To avoid the problem, we employed the TRE-dependent a split-Cre virus combined with c-fos:tTA system (Fig. 3M-N). Although we had a small leak expression under ON-Dox condition when we conducted the long-term labeling in the DG with a split-Cre system (Fig. 3M-N), the leak expression was much smaller than homecage labeling and we clearly observed the CFC-induced increment of cell labeling with ChR2-mCherry in the DG.

Cell Counting

Sixty minutes after the exposure to Context-A or CFC, animals were perfused and their brains were fixed with 4% PFA to detect the c-Fos immunoreactivities in the DG, CA3 and PFC with anti-c-Fos antibody (Santa Cruz Biotechnology, SC-52, 1/1000). Figure 1M-O (PFC) and Figure 2Q (PFC), a sampling of c-Fos^+ cells was conducted throughout PFC (from AP: +1.94 mm to AP: +1.34 mm) in coronal sections for the quantification analysis of the number of c-Fos^+ cells in dorsal medial PFC in each group of mice. Five coronal PFC sections were used to count the number of c-Fos^+ cells and $DAPI^+$ cells in the PFC regions and calculated the percentage of c-Fos^+/ $DAPI^+$ in each groups. In Figure 3D, a sampling of c-Fos^+ cells was conducted throughout dorsal CA3 in sagittal sections for the quantification analysis of the number of c-Fos^+ cells in

CA3 in each group of mice. Ten sagittal hippocampal sections were used to count the number of c-Fos$^+$ cells and DAPI$^+$ cells in CA3 regions and calculated the percentage of c-Fos$^+$/ DAPI$^+$ in each groups. In Figure 4F-K, a sampling of c-Fos$^+$ cells was conducted in anterior BLA (from AP: -1.0 mm to AP: -1.6 mm) in coronal sections for the quantification analysis of the number of c-Fos$^+$ cells in BLA in each group of mice, since fear-related neurons are localized more anterior part of BLA (*44*, *45*). Five coronal BLA sections were used to count the number of c-Fos$^+$ cells and DAPI$^+$ cells in BLA regions. All counting was performed blind as to the group and condition. When we evaluated the reactivation of engram cells by natural recall cues (or non-conditioned cues) in PFC (Fig. 2A-C, Fig. 3E-F), DG (Fig. 3I-L), and BLA (Fig. 4F-K) (we referred in text as overlap experiment), the numbers of H2B-GFP$^+$ cells, c-Fos$^+$ cells and DAPI$^+$ cells in the region of interest (ROI) obtained by the confocal microscopy were counted, and the ratios of c-Fos$^+$ H2B-GFP$^+$ / H2B-GFP$^+$ and the ratio of c-Fos$^+$ H2B-GFP$^-$ / H2B-GFP$^-$ were calculated. Reactivation of hippocampal engram cells by natural cues were previously conducted by several different groups (*20, 29, 32, 46, 47*). Total number of DAPI$^+$ cells studied were 3,984 (Fig. 2C), 7,894 (Fig. 3L), 2,091 (Fig. 3F), and 870 (Fig. 4H, K) cells. Chance level for overlap in BLA (Fig. 4H, K) was calculated as (c-Fos$^+$/DAPI$^+$) x (H2B- GFP$^+$/DAPI$^+$) as previously reported (*48*).

Dendritic Spines Density in PFC and DG Engram Cells

Dendritic spine counting was conducted as previously described (*24, 26*) with minor changes. Engram cells in the PFC and the DG were labelled using c-Fos-tTA-driven synthesis of ChR2–mCherry. The mCherry signal was amplified using immunohistochemistry procedures with anti-RFP antibody (Rockland, 600-401-379, 1/1000), after which fluorescence z-stacks were taken by confocal microscopy using a × 40 objective. Maximum intensity projections were generated using ZEN Black software. Three mice per experimental group were analyzed for dendritic spines. For each mouse, 20–30 dendritic fragments of 10 μm length were quantified (n = 70–110 fragments per group, detail is shown in *Statistics and Sample Sizes*). To measure spine density of DG engram cells, dendritic fragments in the middle molecular layer were selected. For PFC engram cells, apical and basal dendritic fragments were selected. To compute spine density, the number of spines counted on each fragment was normalized by the cylindrical approximation of the surface of the specific fragment. Experiments and analyses were conducted blind to

experimental group. Averages of spines density in the PFC cells and DG cells were comparable with previous reports (*14, 24, 26, 49*).

Optogenetic activation of PFC and DG Engram Cells

In this study, we tested whether activating PFC and DG engram cells labelled by ChR2–eYFP during CFC is sufficient for memory recall at recent and remote time points. For light-induced freezing behavior, a context distinct from the CFC training chamber (Context-B) was used. These were 30 × 25 × 33 cm chambers with white plastic floors, square ceilings, white lighting, and scented with 0.25 % benzaldehyde. Chamber ceilings were customized to hold a rotary joint connected to two 0.32-m patch cords. All mice had patch cords fitted to the optic fiber implant before testing. ChR2 was stimulated at 4 Hz (15 ms pulse width) or 20 Hz (15 ms pulse width) using a 473 nm laser (10–15 mW), for the designated epochs. Testing sessions were 12 min in duration, consisting of four 3 min epochs, with the first and third as light-OFF epochs, and the second and fourth as light-ON epochs. At the end of 12 min, the mouse was detached and returned to its home cage. Floors of chambers were cleaned with 70 % ethanol before test. Freezing counting experiments were conducted double blind to experimental group. Experiments that resulted in significant behavioral effects were replicated three times in the laboratory. Following behavioral protocols, brain sections were prepared to confirm efficient viral labelling in target areas. Animals lacking adequate labelling were excluded before behavior quantification.

TeTX Expression in HPC Engram Cells

To inhibit the synaptic transmission from HPC engram cells after CFC, AAV_9-TRE:TeTX was targeted to bilaterally inject into the hippocampal dentate gyrus of c-fos:tTA mice and the virus was often distributed to not only DG but also CA3 region. To avoid DOX-independent TeTX expression (leak expression) in the HPC, we injected the 100-fold diluted AAV solution with PBS. To examine the effect of TeTX expression in DG engram cells on the reactivation of PFC engram cells at remote timepoint (Fig. 3E-F), we injected the AAV_5-TRE:H2B-GFP into the PFC and AAV_9-TRE:TeTX into the HPC of c-fos:tTA mice. To examine the effect of TeTX expression in DG engram cells on the spine density of the PFC engram cells at remote timepoint (Fig. 3G), we injected the AAV_9-TRE:ChR2-mCherry into the PFC and AAV_9-TRE:TeTX into the HPC of c-fos:tTA mice. To examine the effect of TeTX expression in DG engram cells on

the GCaMP activity of PFC cells at recent and remote timepoint (Fig. 3H), we injected the AAV_5-Syn:GCaMP6f into the PFC and AAV_9-TRE:TeTX into the HPC of c-fos:tTA mice. The c-fos:tTA mice were maintained under the food condition containing 40 mg/kg Dox from their birth.

Monosynaptic Tracing with Rabies Virus

For the monosynaptic retrograde tracing experiment (fig. S5), 150 nl of AAV_5-TRE:HTG (H2BGFP-TVA-G) was stereotaxically delivered into the PFC of c-fos:tTA mice (AP: +1.7 mm, ML, ±0.35 mm, DV, -1.7 mm). Experiments were all conducted in 15–25-week-old male and female mice. The c-fos:tTA mice were maintained under the food condition containing 40 mg/kg Dox from their birth. Mice were single housed post-surgery and throughout the rest of the experiments. In order to open a window of activity-dependent labeling for CFC in Context-A, the mice were then taken off Dox for 24 hours. Animals were exposed to Context-A for 300 s for CFC, and DOX diets were resumed immediately after CFC. One day after CFC, 50 nl of rabies virus, RVΔG-mCherry(EnvA), was injected at the same coordinates, and mice were perfused 3-5 days later.

Calcium Imaging

Calcium imaging from PFC was performed on WT mice in the animal facility during the light cycle. Mice were habituated to human experimenters as well as the experimental room two weeks following AAV injection, microendoscope implant, and baseplate surgeries. Imaging from PFC via microendoscope was previously reported (*50*). Experiments were run in several different pairs of contexts (Fig. 2J). On Day-1, mice were first exposed to Context-B followed by CFC in Context-A. Mice were then re-exposed to both contexts in the same order one day later (Day-2) and 14 days later (Day-15). Ca^{2+} signals from GCaMP6f were imaged during entire exposure periods. The chambers were cleaned with 70 % ethanol between sessions. Immediately before and after imaging sessions, the mouse rested on a pedestal next to the experimental room. Ca^{2+} signals from GCaMP6f were captured at 20 Hz on a miniature microscope. The movie of Ca^{2+} signals was then motion corrected using Inscopix Mosaic software (correction type: translation and rotation; reference region with spatial mean (r = 20 pixels) subtracted, inverted, and spatial mean applied (r = 5 pixels)). Finally, it was processed by ImageJ (dividing each image, pixel by

pixel, by a low-passed (r = 20 pixels) filtered version), and the ΔF/F signal was calculated by Inscopix Mosaic software as previously described (*27, 51*). Cell locations were semi-automatically identified from the stacked image, and selected as small regions of interest (ROIs) (~ 1/3 of cell body size) at the center of the cell bodies. This was done in ImageJ for each processed movie. Approximately 40-80 cells were selected per animal, and their ΔF/F signals were isolated. Calcium traces were calculated at these ROIs for each processed movie, in ImageJ. Calcium events were detected by thresholding (> 3 Standard Deviations from the ΔF/F signal,) at the local maxima of the ΔF/F signal. In Fig 2G-O, total 220 cells in the PFC are monitored from 3 mice. In Fig 3H, total 89 cells in the PFC are monitored from 2 mice. A rate difference index (defined below) was calculated for all cells that had > 10 Ca^{2+} events during exposure to a context. To define the shock-responding cells in PFC, we calculated the averaged frequency of each PFC cell during Context-A (5 min), Context-B (5 min, excluding shock periods), and Shock periods in Context-B (2 min) on Day-1. If the Averaged frequency in shock-period was 4 times higher than that in Context-A and Context-B (before shock), the cells are identified as shock responding (SR) cells.

Rate Difference Index of Ca^{2+} Events

We used the following score to determine the score of "context preference" in each single cell:

$$Rate\ Difference\ \ Index = \frac{n_{\text{events,X}} - n_{\text{events,Y}}}{n_{\text{events,X}} + n_{\text{events,Y}}}$$

Where $n_{\text{events,X}}$ is the number of Ca^{2+} events in context *X*. Similar definition for $n_{\text{events,Y}}$.

The rate difference score was calculated for every cell in each animal for Context-A versus Context-B on Day-1, Day-2 and Day-15 to evaluate the preference of Ca^{2+} activity in different contexts. In Figure 2, we displayed the cumulative probability of the rate difference indices for different contexts (A vs B) on Day-1, Day-2 and Day-15. When the distribution shifts to right, this indicates a larger change in the number of Ca^{2+} events and higher median rate difference index.

Statistical Analysis

GraphPad Prism version 6.01 for Windows, GraphPad Software, La Jolla California USA was used for statistical analysis. All data are presented as mean ± SEM. N indicates number of animals. n indicates number of cells or spines. Comparisons between two-group data were analyzed by two-tailed unpaired t-test or two-tailed paired t-test. Comparisons of distribution data between two-groups were analyzed by Kolmogorov–Smirnov (KS) test. Multiple group comparisons were assessed using a one-way, two-way (ANOVA), followed by the post-hoc Tukey-Kramer test when significant main effects or interactions were detected. The null hypothesis was rejected at the $P < 0.05$ level. Data met assumptions of statistical tests. Sample sizes were chosen on the basis of previous studies (*17, 19, 24, 26, 27, 29, 35*).

Supplemental Figures

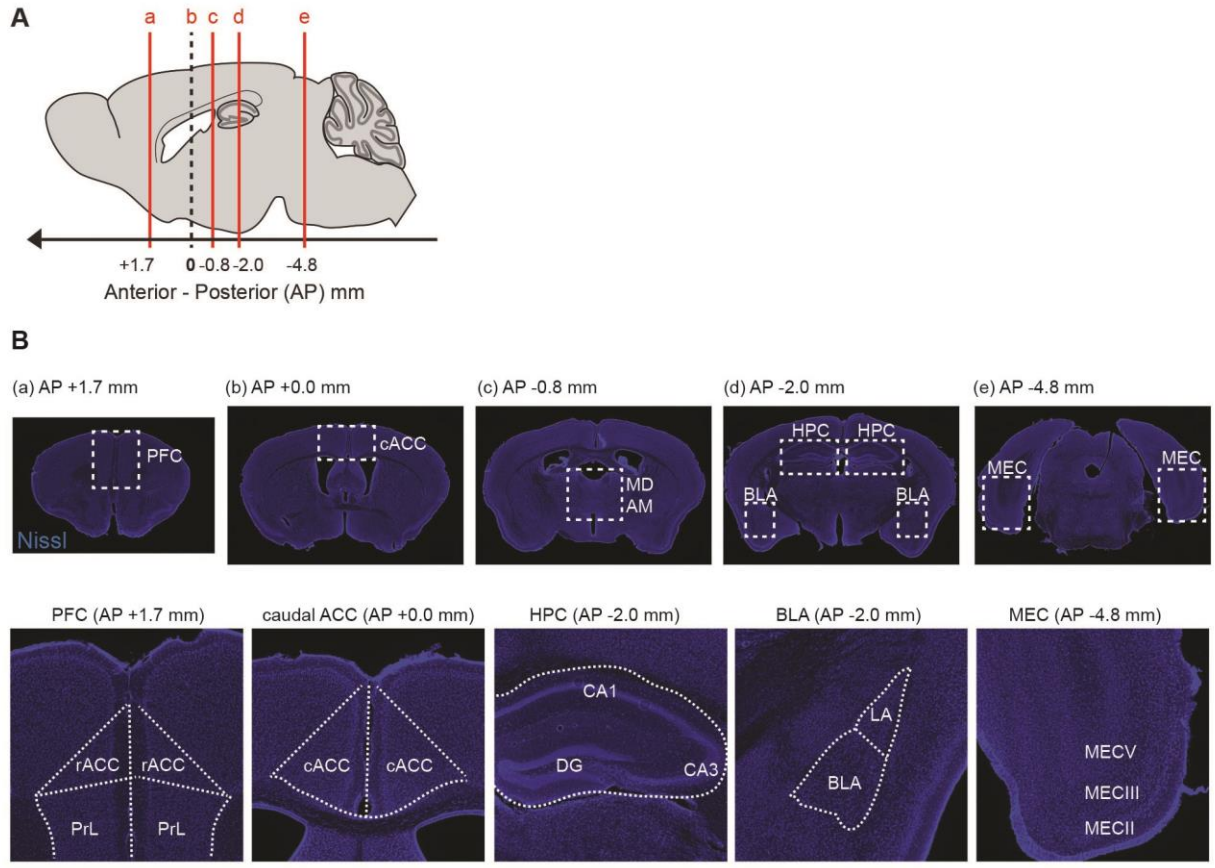

Fig. S1 Brain region references for systems consolidation of memory.

(A) Sagittal section of mouse brain. **(B)** Coronal sections at each AP positions (AP = +1.7mm; PFC, AP = 0.0 mm; caudal part of ACC (cACC), AP = -0.8 mm; MD, AM, AP = -2.0 mm; HPC, BLA, AP = -4.8 mm; MEC). PFC includes rostral part of ACC (rACC) and prelimbic cortex (PrL). Hippocampus (HPC) includes DG, CA3 and CA1. LA; lateral amygdala, BLA; basolateral amygdala.

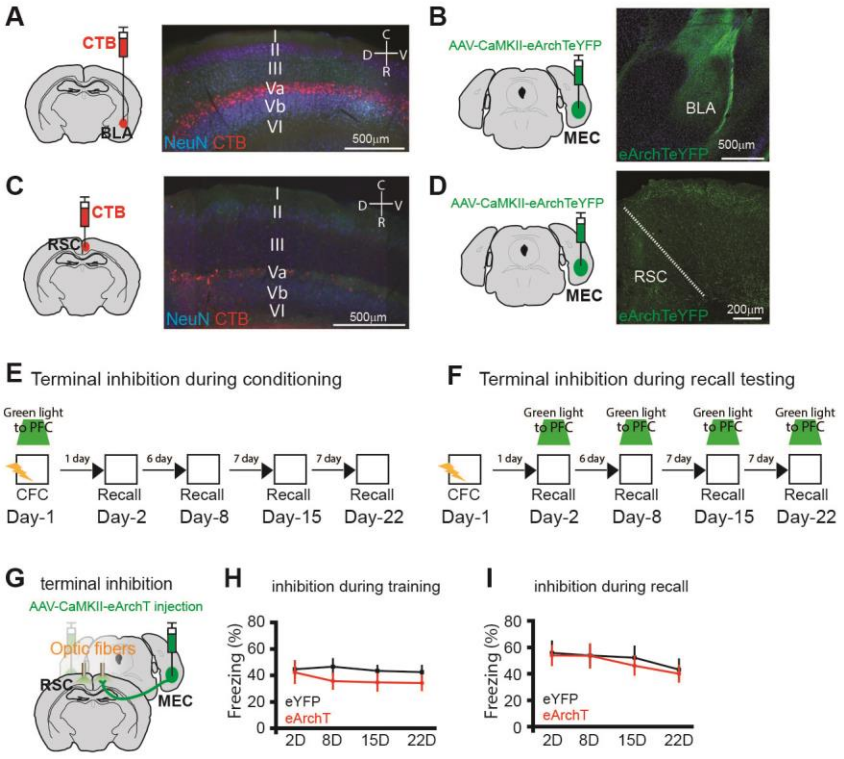

Fig. S2

MEC-Va input to RSC during the conditioning or testing periods is dispensable for contextual fear memory. (A-B) CTB was injected into BLA. Sagittal section of MEC visualized with CTB-labeled cell bodies (red) and immunostained with anti-NeuN (blue) (N = 10 mice) (A). Coronal sections of BLA visualized with MECVa axons by eYFP (green) (B). **(C-D)** CTB was injected into RSC. Sagittal section of MEC visualized with CTB-labeled cell bodies (red) and immunostained with anti-NeuN (blue) (N = 5 mice) (C). Coronal sections of RSC visualized with MECVa axons by eYFP (green) (D). **(E-F)** Experimental schedules. **(G-I)** Mice were injected with the AAV_8-CaMKII:eArchT-eYFP bilaterally into MEC and implanted with an optic fiber bilaterally into the RSC (G). Time courses of freezing during recall tests on 1 day (Day-2), 7 days (Day-8), 14 days (Day-15) and 21 days (Day-22) after CFC. Green light was shone into RSC during conditioning (H) or testing (I). **(H)** eYFP; N = 8 mice, eArchT; N = 8 mice. There were no difference between eYFP and eArchT groups in freezing response on Day-2 ($t14 = 0.23$, $P = 0.82$), Day-8 ($t14 = 1.21$, $P = 0.25$), Day-15 ($t14 = 1.03$, $P = 0.32$) and Day-22 ($t14 = 0.98$, $P = 0.34$), analyzed by two-tailed unpaired t-test. **(I)** eYFP; N = 6 mice, eArchT; N = 6 mice. There were no difference between eYFP and eArchT groups in freezing response on Day-2 ($t10 = 0.16$, $P = 0.88$), Day-8 ($t10 = 0.02$, $P = 0.99$), Day-15 ($t10 = 0.52$, $P = 0.62$) and Day-22 ($t10 = 0.31$, $P = 0.77$), analyzed by two-tailed unpaired t-test. Error bars, mean ± s.e.m.

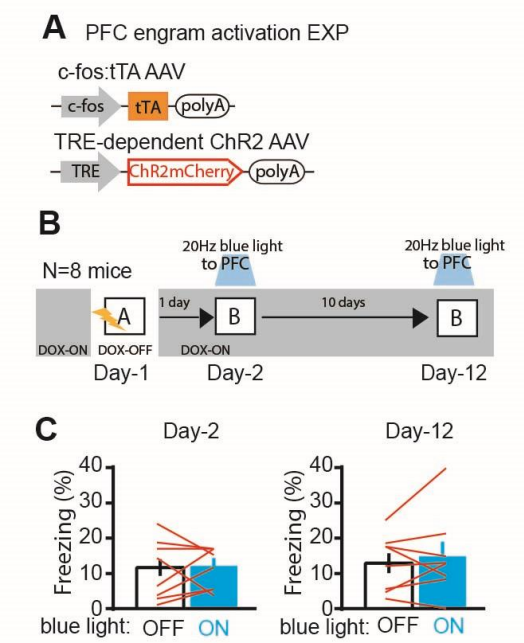

Fig. S3

Conventional 20 Hz blue light stimulation of ChR2-mCherry-expressing cells in the PFC does not induce the freezing behavior. (A) Virus-mediated engram labelling strategy using a cocktail of AAV_9-c-fos:tTA and AAV_9-TRE:ChR2-mCherry into PFC. **(B)** Experimental schedule for optogenetic activation of c-Fos expressed cells in PFC. **(C)** Freezing by blue light stimulation 1 day and 11 days after CFC. Average freezing for light-off and light-on epoch (N = 8 mice). There were no difference in freezing score between light-off and light-on epochs on Day-2 ($t7$ = -0.7, P = 0.51) and Day-12 ($t7$ = -0.77, P = 0.47), analyzed by two-tailed paired t-test. Error bars, mean ± s.e.m.

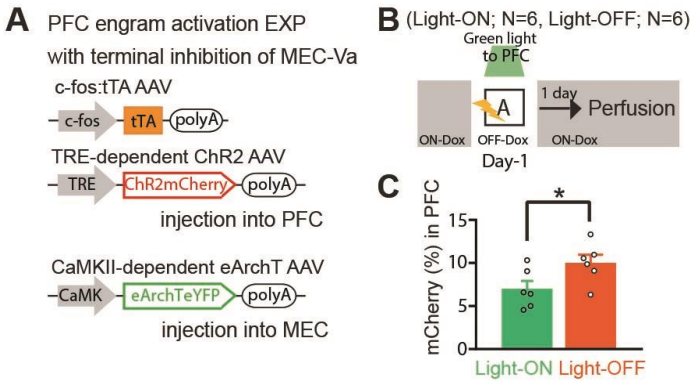

Fig. S4 Terminal inhibition of MEC-Va fibers at the PFC reduced the number of ChR2-mCherry^{+} cells in the PFC

(A) Virus-mediated engram labelling strategy using a cocktail of AAV_9-c-fos:tTA and AAV_9-TRE:ChR2-mCherry into PFC with injection of AAV_8-CaMKII-eArchTeYFP into the MEC. **(B)** Experimental schedule. **(C)** Percentages of mCherry^{+} cells in PFC of green light-ON group and green light-OFF group. There was a significant difference in the percentages of mCherry^{+} cells in the PFC between green light-ON group (N=6 mice) and green light-OFF group (N=6 mice) ($t10 = -2.29$, $P = 0.045$).

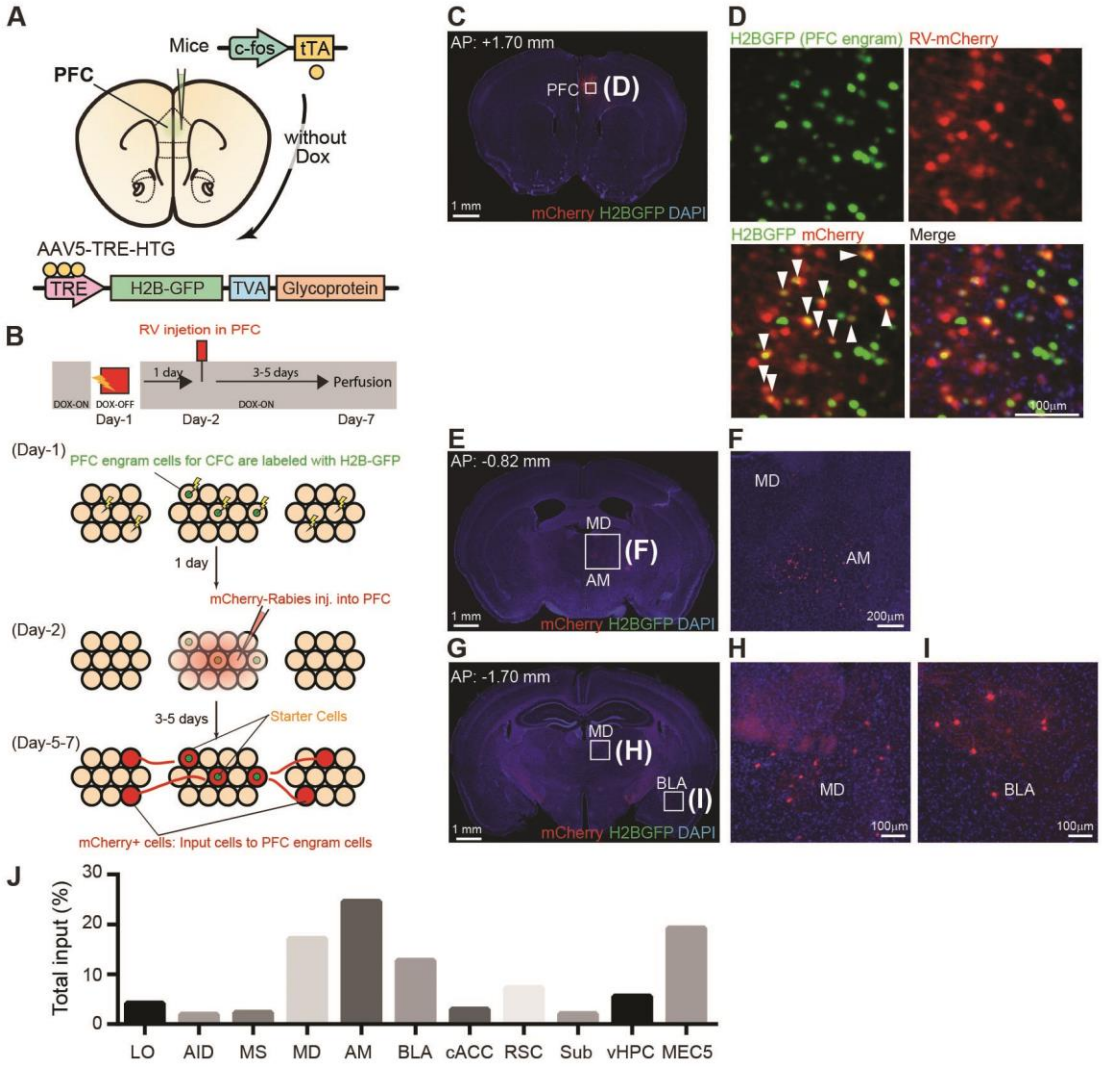

Fig. S5

Identification of monosynaptic inputs onto PFC engram cells. (A-B) Experimental schedules. To visualize the brain areas that provide monosynaptic inputs to PFC engram cells, we used TRE-dependent AAV (AAV_5-TRE-HTG) (Miyamichi et al., 2011) encoding H2B-GFP, the avian cell-surface receptor TVA, and the rabies virus glycoprotein (G), and injected this stereotaxically into the PFC area of c-fos-tTA transgenic mice. One day after CFC while mice are DOX-Off, a deletion-mutant rabies virus encoding mCherry and packaged with the TVA-specific envelope protein EnvA (RVΔG-mCherry(EnvA)), was injected into the same area and the brain was analyzed 3-5 days later (B). **(C-I)** With this method, starter cells of PFC engram cells will be labeled by both mCherry (red) and H2B-GFP (green) and will therefore appear yellow (arrow heads), while the cells that are directly presynaptic to PFC engram cells will be labeled by mCherry only and hence appear red (B-D). $mCherry^+$ cells were observed not only in MEC-Va (Fig. 1W), but also in medial dorsal thalamus (MD) (E, F, G, H), anteromedial thalamus (AM) (G, H), and BLA (G, I). **(J)** Distribution of mCherry+ cells in the brain (n=770 $mCherry^+$ cells). LO; lateral orbital cortex, AID; agranular insular cortex, MS; medial septum, Sub; subiculum, vHPC; ventral hippocampus.

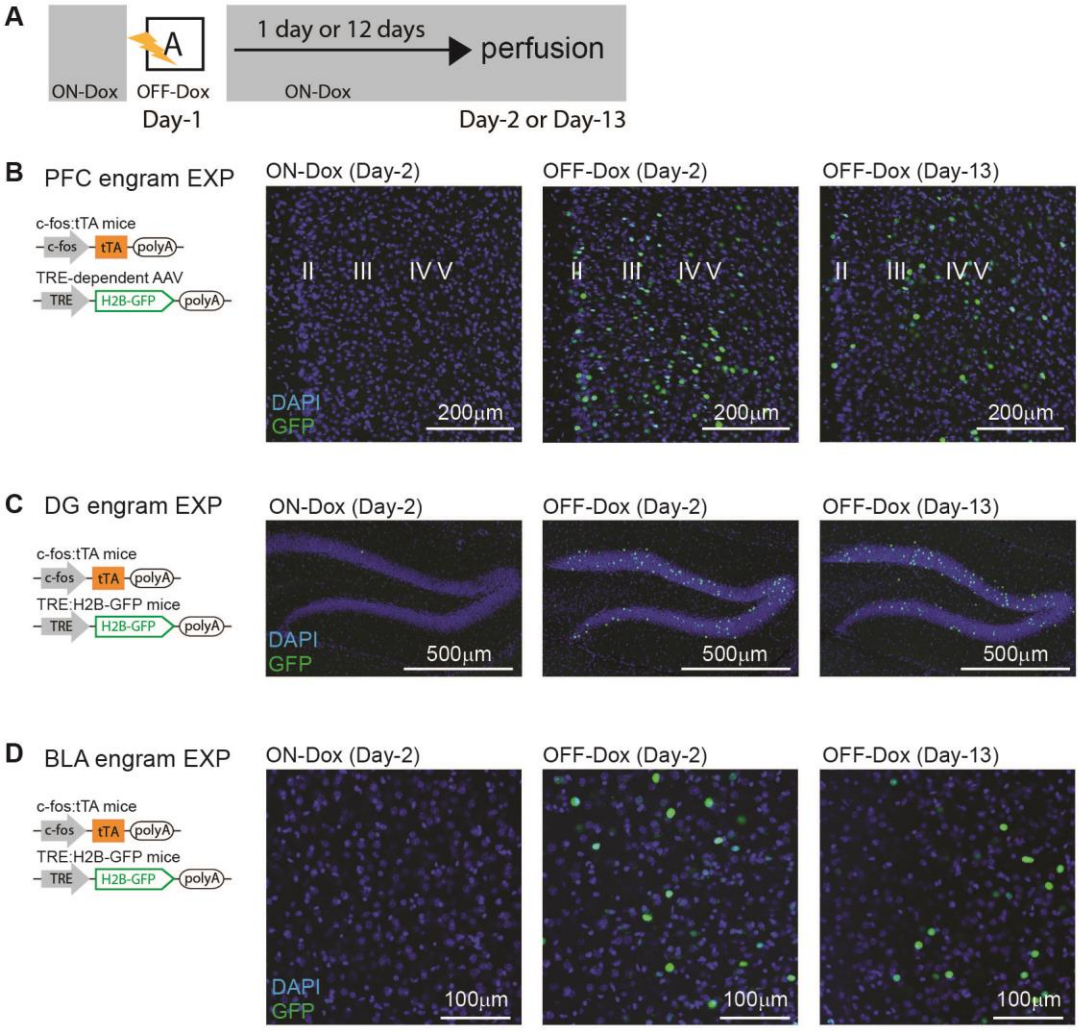

Fig. S6

Engram cell labeling in PFC, DG and BLA with H2B-GFP is DOX-dependent. (A) Experimental schedule. **(B)** PFC engram cells labelling injecting AAV_9-TRE:H2B-GFP into PFC of c-fos:tTA transgenic mice. Coronal sections of PFC visualized with H2B-GFP (green) and DAPI (blue) under ON-Dox and OFF-Dox conditions (1 day and 12 days after CFC). **(C-D)** Transgenic strategy of engram labelling using c-fos:tTA transgenic crossed with TRE:H2B-GFP transgenic mice. Coronal sections of DG (C) and BLA (D) visualized with H2B-GFP (green) and DAPI (blue) under ON-Dox and OFF-Dox conditions (1 day and 12 days after CFC) (N = 3 mice, each group).

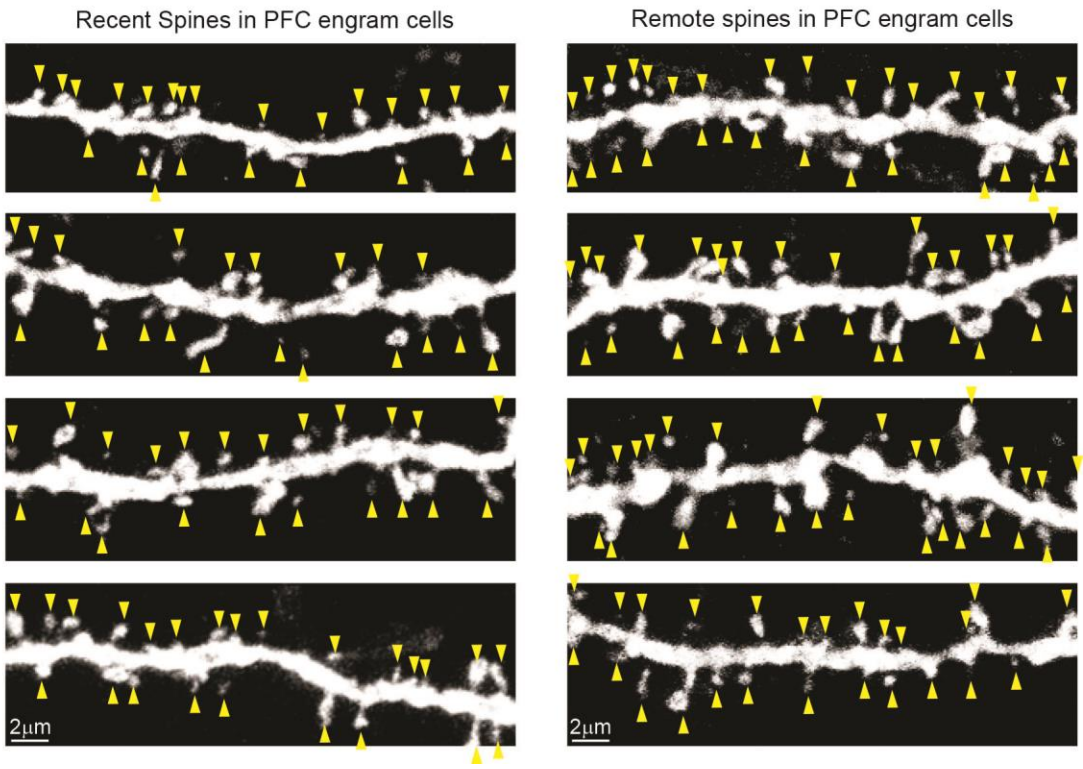

Fig. S7

Confocal Images of Dendritic Spines of PFC memory engram cells in recent and remote time points. Four series of confocal images of dendritic spines of recent PFC engrams (left) and remote PFC engrams (right) group. Arrow heads (yellow) indicate dendritic spines.

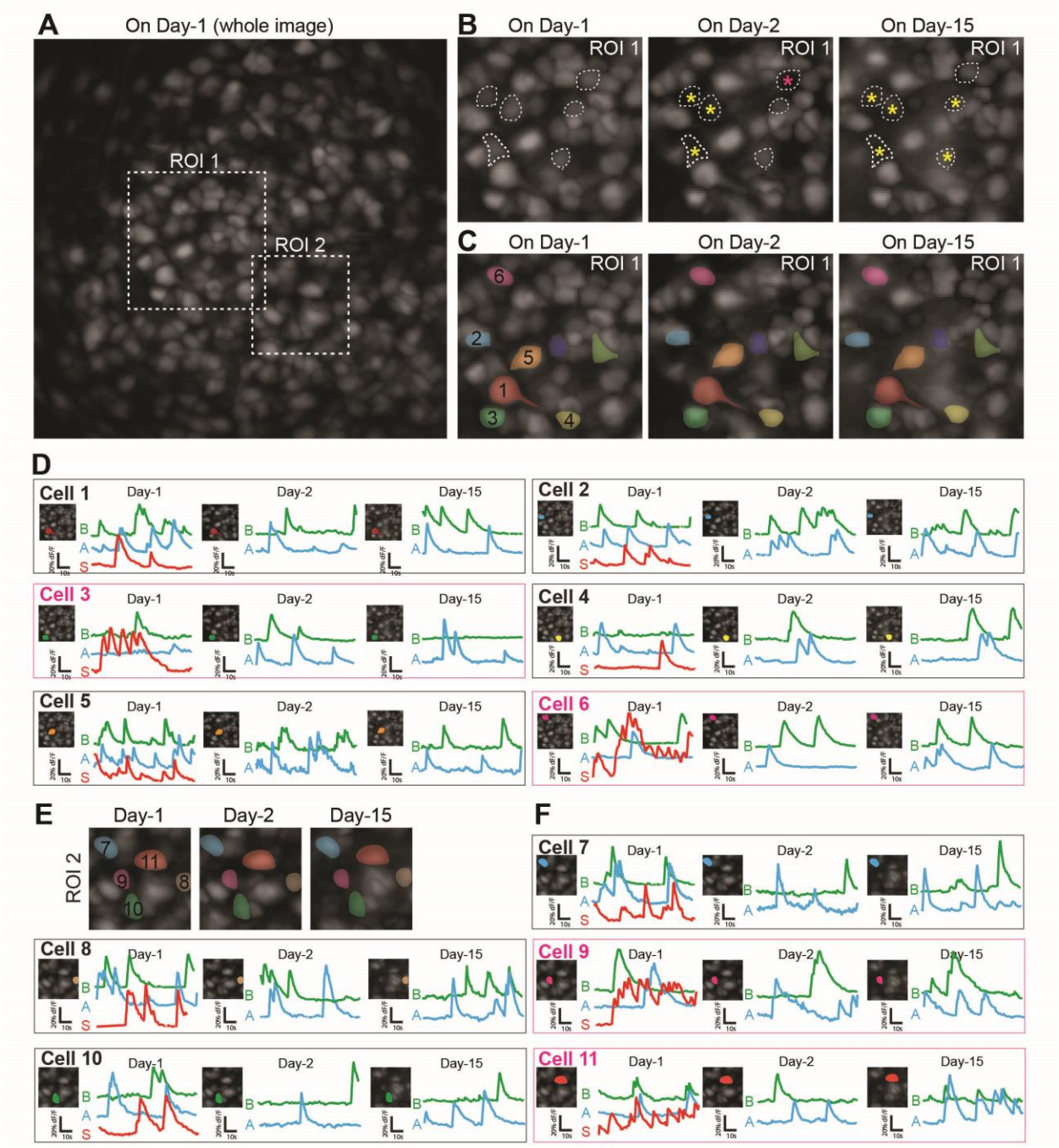

Fig. S8 Longitudinal imaging of PFC cells during CFC, recent and remote recall (A) Stacked image acquired from PFC through the microendoscope on Day-1. Region of interest (ROI). **(B)** Some cells disappear during 2 weeks imaging. Six dot lined cells were active on Day-1, but with time they lost their GCaMP6 activity. In this case, it is difficult to case individual cells through 2 weeks. Asterisks mean disappear of cells. **(C)** Stacked image acquired from PFC in ROI1 through the microendoscope on Day-1, Day-2 and Day-15. Six colored cells indicate that was successfully cased through 2 weeks. Labeled 8 cells constantly showed their GCaMP activity for 2 weeks, were successfully cased individual cells longitudinally. **(D)** GCaMP activity of PFC cells during Day-1, Day-2, and Day-15 in ROI1. B; Context-B, A; Context-A, S; shock

period. Cell 3 and Cell 6 were Shock Responding cells. **(E)** Stacked image acquired from PFC in ROI2 through the microendoscope on Day-1, Day-2 and Day-15. Five colored cells indicate that was successfully cased through 2 weeks. **(F)** GCaMP activity of 5 PFC cells during Day-1, Day-2, and Day-15 in ROI 2. B; Context-B, A; Context-A, S; shock period. Cell 9 and Cell 11 were Shock Responding cells.

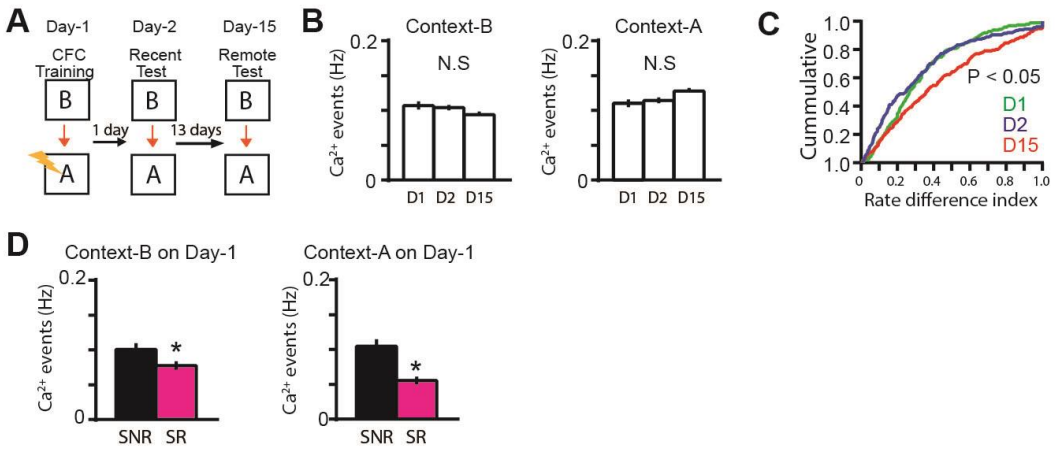

Fig. S9

GCaMP activity of PFC cells during CFC and recall periods. (A) Experimental schedule. **(B)** Average Ca^{2+} event frequency of PFC cells during Context-B and Context-A on Day1, 2 and15. **(C)** Cumulative probability of rate difference index of Ca^{2+} activity of PFC cells during Context-B and Context-A on Day1 (median; 0.2683), Day-2 (median; 0.2389) and Day-15 (median; 0.3560) (n = 220 cells, N = 3 mice). There were significant differences in the cumulative distribution curves of a rate difference index (see Methods) between Day-1 conditioning and Day-15 recall, and between Day-2 recall and Day-15 recall analyzed by Kolmogorov-Smirnov Comparison, *P = 0.001. **(D)** Average Ca^{2+} event frequency of SNR cells (n = 28 cells, N = 3 mice) and SR cells (n = 26 cells, N = 3 mice) during Context-B and Context-A on Day-1 (not including the shock delivery period). There was significant difference between SR and SNR groups in Context-B ($t52$ = 2.11, P = 0.039) and Context-A ($t52$ = 3.99, P = 0.0002). *P < 0.05, by two-tailed t-test. N.S means not significant. Error bars, mean ± s.e.m.

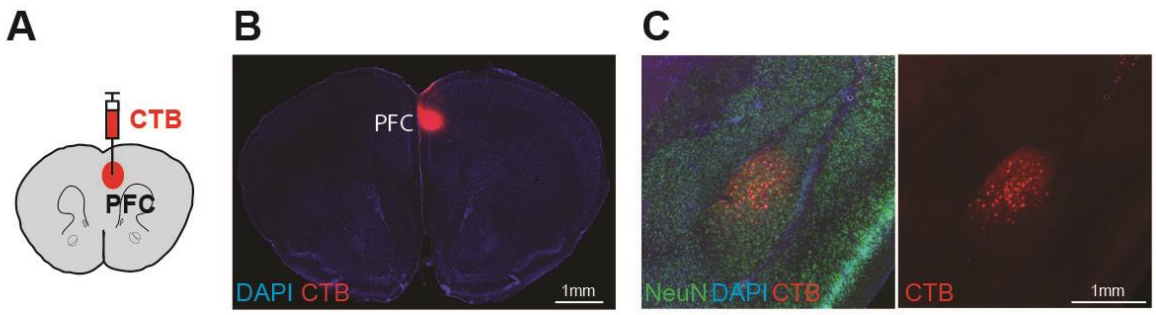

Fig. S10
BLA cells project to PFC. (A) Experimental schedule. **(B-C)** CTB was injected into PFC (B). Coronal section of BLA visualized with CTB-labeled cell bodies (red) and immunostained with anti-NeuN (green) and DAPI (blue) (N = 4 mice) (C).

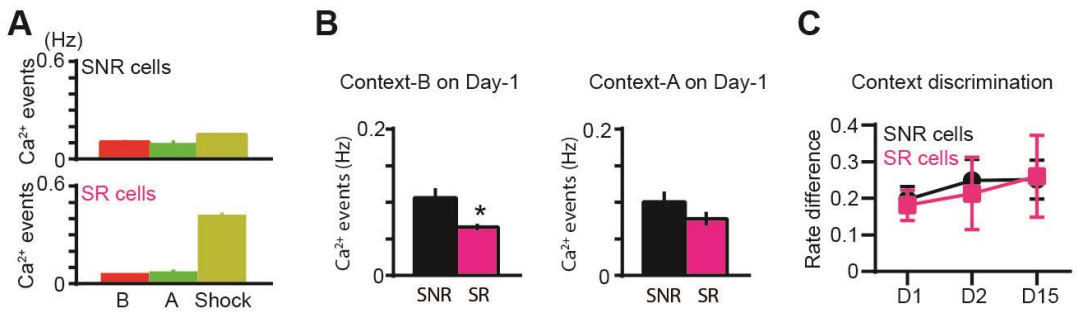

Fig. S11

GCaMP activity of PFC cells during CFC and recall periods with TeTX expression in HPC engram cells. (A) Average Ca^{2+} event frequency of SNR cells and SR cells during Context-B, Context-A and following shock periods in Context-A on Day1 under the condition which HPC engram cells express TeTX. **(B)** Average Ca^{2+} event frequency of SNR cells (n = 10 cells, N = 2 mice) and SR cells (n = 8 cells, N = 2 mice) during Context-B and Context-A on Day-1 (not including the shock delivery period). There was significant difference between SR and SNR groups in Context-B ($t16$ = 2.62, P = 0.018) but not in Context-A ($t16$ = 1.29, P = 0.21), analyzed by two-tailed unpaired t-test. *P < 0.05, by two-tailed unpaired t-test. **(C)** Average rate difference index of Ca^{2+} activity during Context-B and Context-A of SNR cells (black, n = 10 cells, N = 2 mice) and SR cells (pink, n = 8 cells, N = 2 mice) on Day-1, Day-2 and Day-15. There was no significant rate difference between SNR and SR cells on Day-1 ($t16$ = 0.29, P = 0.78), Day-2 ($t16$ = 0.33, P = 0.74) and Day-15 ($t16$ = -0.08, P = 0.94), analyzed by two-tailed unpaired t-test. Error bars, mean ± s.e.m.

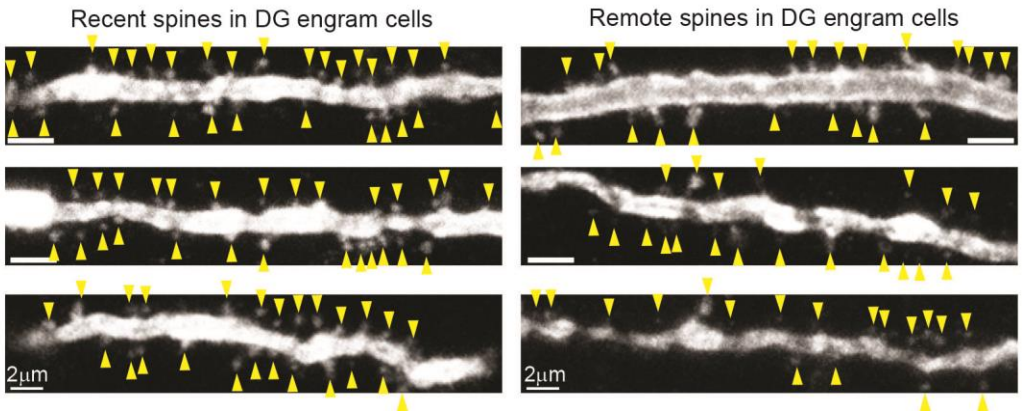

Fig S12

Confocal Images of Dendritic Spines of hippocampal DG memory engram cells in recent and remote time points. Three series of confocal images of dendritic spines of recent DG engrams (left) and remote DG engrams (right) group. Arrow heads (yellow) indicate dendritic spines.

Statistics and Sample Sizes

Figure 1:

(A) CTB injection into PFC (N = 10 mice). **(B)** Coronal sections of PFC with MECVa axons visualized by eYFP (N = 10 mice). **(C, D)** CTB injection into BLA (N = 10 mice). **(F)** eYFP; N = 10 mice, eArchT; N= 10 mice. There were no difference between eYFP and eArchT groups in freezing response on Day-2 ($t18 = -0.28$, P = 0.78) and Day-8 ($t18 = 0.39$, P = 0.70) analyzed by two-tailed unpaired t-test. However, there were significant differences between eYFP and eArchT groups in freezing response on Day-15 ($t18 = 4.85$, P = 0.0001) and Day-22 ($t18 = 2.96$, P = 0.008), analyzed by two-tailed unpaired t-test. **(G)** eYFP; N = 8 mice, eArchT; N = 10 mice. There were no difference between eYFP and eArchT groups in freezing response on Day-2 ($t16 = 0.026$, P = 0.98), Day-8 ($t16 = 0.74$, P = 0.47), Day-15 ($t16 = -0.82$, P = 0.43) and Day-22 ($t16 = 0.71$, P = 0.49), analyzed by two-tailed unpaired t-test. **(H)**, CTB injection into ACC (N = 8 mice). **(I)** Coronal sections of ACC with MECVa axons visualized by eYFP (N = 10 mice). **(K)** eYFP; N = 10 mice, eArchT; N = 12 mice. There were no difference between eYFP and eArchT groups in freezing response on Day-2 ($t20 = 1.06$, P = 0.30), Day-8 ($t20 = 0.96$, P = 0.35), Day-15 ($t20 = 1.56$, P = 0.14) and Day-22 ($t20 = 1.49$, P = 0.15), analyzed by two-tailed unpaired t-test. **(L)** eYFP; N= 8 mice, eArchT; N= 8 mice. There were no difference between eYFP and eArchT groups in freezing response on Day-2 ($t14 = -0.84$, P = 0.41), Day-8 ($t14 = 0.05$, P = 0.96), Day-15 ($t14 = 0.15$, P = 0.88) and Day-22 ($t14 = 0.43$, P = 0.67), analyzed by two-tailed unpaired t-test. **(O)** HC; N = 4 mice, CTX; N = 4 mice, CFC with eYFP; N = 4 mice, and CFC with eArchT; N = 4 mice. There was significant differences in the percentage of c-Fos+ cells in the PFC among the 4 groups ($F(3, 12) = 5.425$, P = 0.013, one-way ANOVA). Tukey-Kramer test revealed there were significant difference between HC and CFC-eYFP (P = 0.016) and between CFC-eYFP and CFC-eArchT (P = 0.03) **(Q)** Coronal section of PFC visualized with ChR2-mCherry of ON-DOX (N = 3 mice), OFF-DOX (N = 3 mice), and OFF-DOX (N = 3 mice) conditions. **(S)** N = 6 mice. There were significant differences between light-OFF and light-ON conditions in freezing response on Day-2 ($t5 = -2.89$, P = 0.034) and Day-12 ($t5 = -4.69$, P = 0.005), analyzed by two-tailed paired t-test. **(U)** N = 5 mice. There was no difference between light-OFF and light-ON conditions in freezing response on Day-2 ($t4 = -0.45$, P = 0.67)

and Day-12 ($t4$ = -1.55, P = 0.19), analyzed by two-tailed paired t-test. **(W)**. Distribution of $mCherry^+$ cells in the MEC (n = 212 $mCherry^+$ cells, N = 3 mice).

Figure 2:

(C) N = 5 mice, each group, There was no difference in percentages of c-Fos^+ cells between GFP^+ and GFP^- cells in the condition of Recent A-A (N = 5 mice, total number of $DAPI^+$ cells was 1,155 cells, $t8$ = -0.82, P = 0.43), Recent A-B (N = 5 mice, total number of $DAPI^+$ cells was 1,100 cells, $t8$ = -0.54, P = 0.60) and Remote A-B (N = 5 mice, total number of $DAPI^+$ cells was 830 cells, $t8$ = -0.52, P = 0.61), but a significant difference in the condition of Remote A-A (N = 5 mice, total number of $DAPI^+$ cells was 889 cells, $t8$ = 3.45, P = 0.0087), analyzed by two-tailed unpaired t-test. **(E)** Day-2; n = 507 spines, 62 fragments of dendrites, N = 3 mice, Day-12; n = 587 spines, 62 fragments of dendrites, N = 3 mice, There was significant difference in spine density between recent (Day-2) and remote (Day-12) conditions, analyzed by Kolmogorov-Smirnov Comparison (D = 0.2419, P = 0.044). **(F)** N = 10 mice. There were significant differences between green light-OFF and green light-ON conditions in freezing response on Day-12 ($t9$ = 3.05, P = 0.013), but not on Day-2 ($t9$ = 1.04, P = 0.32), analyzed by two-tailed paired t-test. **(G-O)** Total 220 cells in the PFC are monitored from 3 mice. **(L-O)** SNR cells; n = 28 cells, N = 3 mice, SR cells; n = 26 cells, N = 3 mice. **(M)** There were no difference in Ca^{2+} event frequency between Context-B and Context-A on Day-1 ($t27$ = -0.30, P = 0.77), Day-2 ($t27$ = -0.49, P = 0.63), and Day-15 ($t27$ = 1.42, P = 0.17), analyzed by two-tailed paired t-test. **(N)** There was no difference in Ca^{2+} event frequency between Context-B and Context-A on Day-2 ($t25$ = 1.13, P = 0.27), but significant difference on Day-15 ($t25$ = 2.59, P = 0.016), analyzed by two-tailed paired t-test. **(O)** There were no difference in rate difference index between SNR cells and SR cells on Day-1 ($t52$ = -0.68, P = 0.50), Day-2 ($t52$ = 1.06, P = 0.29), but was significant difference on Day-15 ($t52$ = -2.19, P = 0.03), analyzed by two-tailed unpaired t-test. **(P)** Coronal sections of PFC visualized with BLA axons by eYFP (N = 4 mice). **(Q)** HC; N = 4 mice, Shock; N = 4 mice, CFC with eYFP; N = 4 mice, and CFC with eArchT; N = 4 mice, There was significant difference in the percentage of c-Fos^+ cells in the PFC among the 4 groups ($F(3, 12)$ = 5.435, P = 0.014, one-way ANOVA). Tukey-Kramer test revealed there were significant difference between HC and CFC-eYFP (P = 0.014) and between CFC-eYFP and CFC-eArchT (P = 0.033). **(R)** eYFP; N = 6 mice, eArchT; N = 6 mice. There were no difference between eYFP

and eArchT groups in freezing response on Day-2 ($t10 = 0.66$, P = 0.74), Day-8 ($t10 = 0.30$, P = 0.77) and Day-15 ($t10 = 1.96$, P = 0.08), analyzed by two-tailed unpaired t-test. However, there was a significant differences between eYFP and eArchT groups in freezing response on Day-22 ($t10 = 2.35$, P = 0.04), analyzed by two-tailed unpaired t-test.

Figure 3:

(B-C) Sagittal sections of HPC visualized with anti-VAMP2 in ON-Dox (B) and OFF-Dox (C), N = 3 mice, each group. **(D)** HC; N = 4 mice, blue-light-ON mice with eYFP; N = 4 mice, and blue-light-ON mice with TeTX; N = 5 mice. There was significant difference in the freezing responses among the 4 groups (F(3, 10) = 7.119, P = 0.012, one-way ANOVA). Tukey-Kramer test revealed there were significant difference between HC and DG-Stim (P = 0.013) and between DG-Stim with eYFP and TeTX (P = 0.039). **(F)** N = 5 mice, each group. There was a significant difference in percentages of c-Fos$^+$ cells between GFP$^+$ and GFP$^-$ cells in eYFP control group (N = 5 mice, total number of DAPI$^+$ cells was 1,051 cells, $t8 = 2.37$, P = 0.045), but there was no difference in TeTX group (N = 5 mice, total number of DAPI$^+$ cells was 1,040 cells, $t8 = 0.87$, P = 0.40), analyzed by two-tailed unpaired t-test. **(G)** eYFP; n = 1,020 spines, 104 fragments of dendrites, N = 3 mice, TeTX; n = 809 spines, 104 fragments of dendrites, N = 3 mice. There was a significant difference in spine density between eYFP and TeTX groups, analyzed by Kolmogorov-Smirnov Comparison (D = 0.2981, P = 0.0001). **(H)** In SNR cells (n = 10 cells, N= 2 mice), there were no difference in Ca^{2+} event frequency between Context-B and Context-A on Day-1 ($t9 = 0.42$, P = 0.69), Day-2 ($t9 = -0.31$, P = 0.76) and Day-15 ($t9 = 0.24$, P = 0.81), analyzed by two-tailed paired t-test. In SR cells (n = 8 cells, N = 2 mice), there were no difference in Ca^{2+} event frequency between Context-B and Context-A on Day-1 ($t7 = -1.02$, P = 0.34), Day-2 ($t7 = -0.35$, P = 0.74) and Day-15 ($t7 = -0.53$, P = 0.61), analyzed by two-tailed paired t-test. **(L)** There were no difference in percentages of c-Fos$^+$ cells between GFP$^+$ and GFP$^-$ cells in the condition of Recent A-B (N = 5 mice, total number of DAPI$^+$ cells was 1,568 cells, $t8 = -0.57$, P = 0.59) and Remote A-B (N = 5 mice, total number of DAPI$^+$ cells was 1,749 cells, $t8 = -0.42$, P = 0.68), but there were significant difference in the condition of Recent A-A (N = 5 mice, total number of DAPI$^+$ cells was 2,220 cells, $t8 = 3.02$, P = 0.017) and Recent A-A (N = 5 mice, total number of DAPI$^+$ cells was 2,357 cells, $t10 = -2.24$, P = 0.049), analyzed by two-tailed unpaired t-test. **(N)** Coronal sections of DG visualized with ChR2-mCherry (red) under

ON-Dox and OFF-Dox conditions (N = 3 mice, each group). **(O)** Day-5 (recent); n = 623 spines, 60 fragments of dendrites, N = 3 mice, Day-15 (remote); n = 423 spines, 50 fragments of dendrites, N = 3 mice. There was a significant difference in spine density between recent and remote groups, analyzed by Kolmogorov-Smirnov Comparison (D = 0.26, P = 0.041). **(Q)** N = 4 mice, There were significant difference between blue light-OFF and light-ON conditions in freezing response on Day-5 ($t3$ = -4.75, P = 0.018) and Day-15 ($t3$ = -4.57, P = 0.02), analyzed by two-tailed paired t-test.

Figure 4:

(A) Coronal sections of BLA visualized with MECVa axons by eYFP (N = 4 mice). **(B)** eYFP; N = 12 mice, eArchT; N = 12 mice. There were significant differences between eYFP and eArchT groups in freezing response on Day-2 ($t22$ = 3.28, P = 0.003), Day-8 ($t22$ = 3.72, P = 0.001), Day-15 ($t22$ = 2.45, P = 0.03) and Day-22 ($t22$ = 2.39, P = 0.03), analyzed by two-tailed unpaired t-test. **(C)** eYFP; N = 10 mice, eArchT; N = 10 mice. There were significant differences between eYFP and eArchT groups in freezing response on Day-2 ($t18$ = 2.80, P = 0.01) and Day-8 ($t18$ = 3.80, P = 0.001), but no difference on Day-15 ($t18$ = 0.96, P = 0.35) and Day-22 ($t18$ = 0.95, P = 0.35), analyzed by two-tailed unpaired t-test. **(D)** Coronal sections of BLA visualizing axons of PFC engram cells with eYFP (N = 3 mice). **(E)** N = 10 mice. There was a significant difference between green light-OFF and green light-ON conditions in freezing response on Day-12 ($t9$ = 2.80, P = 0.02), but not on Day-2 ($t9$ = 0.72, P = 0.42), analyzed by two-tailed paired t-test compared to chance level. **(H)** N = 5 mice, each group. Chance level for overlap in BLA was calculated as (c-Fos$^+$/DAPI$^+$) x (H2B- GFP$^+$/DAPI$^+$). There were significant differences in the percentages of c-Fos$^+$ GFP$^+$ cells in BLA in recent group (Day-2; N = 5 mice, total number of DAPI$^+$ cells was 216 cells, $t4$ = -3.37, P = 0.028) and remote group (Day-13; N = 5 mice, total number of DAPI$^+$ cells was 219 cells, $t4$ = -2.83, P = 0.047) by two-tailed paired t-test. **(K)** N = 5 mice, each group. There were significant differences in the percentages of c-Fos$^+$ GFP$^+$ cells in BLA in recent group (Day-4; N = 5 mice, total number of DAPI$^+$ cells was 218 cells, $t4$ = -2.83, P = 0.047) and remote group (Day-14; N = 5 mice, total number of DAPI$^+$ cells was 213 cells, $t4$ = -4.97, P = 0.008) by two-tailed paired t-test.

References and Notes

1. D. Marr, Simple memory: A theory for archicortex. *Philos. Trans. R. Soc. Lond. B Biol. Sci.* **262**, 23–81 (1971). doi:10.1098/rstb.1971.0078 Medline

2. L. R. Squire, Mechanisms of memory. *Science* **232**, 1612–1619 (1986). doi:10.1126/science.3086978 Medline

3. J. J. Kim, M. S. Fanselow, Modality-specific retrograde amnesia of fear. *Science* **256**, 675–677 (1992). doi:10.1126/science.1585183 Medline

4. J. L. McClelland, B. L. McNaughton, R. C. O'Reilly, Why there are complementary learning systems in the hippocampus and neocortex: Insights from the successes and failures of connectionist models of learning and memory. *Psychol. Rev.* **102**, 419–457 (1995). doi:10.1037/0033-295X.102.3.419 Medline

5. L. Nadel, M. Moscovitch, Memory consolidation, retrograde amnesia and the hippocampal complex. *Curr. Opin. Neurobiol.* **7**, 217–227 (1997). doi:10.1016/S0959-4388(97)80010-4 Medline

6. D. Tse, R. F. Langston, M. Kakeyama, I. Bethus, P. A. Spooner, E. R. Wood, M. P. Witter, R. G. M. Morris, Schemas and memory consolidation. *Science* **316**, 76–82 (2007). doi:10.1126/science.1135935 Medline

7. J. L. McClelland, Incorporating rapid neocortical learning of new schema-consistent information into complementary learning systems theory. *J. Exp. Psychol. Gen.* **142**, 1190–1210 (2013). doi:10.1037/a0033812 Medline

8. G. Buzsáki, The hippocampo-neocortical dialogue. *Cereb. Cortex* **6**, 81–92 (1996). doi:10.1093/cercor/6.2.81 Medline

9. A. G. Siapas, M. A. Wilson, Coordinated interactions between hippocampal ripples and cortical spindles during slow-wave sleep. *Neuron* **21**, 1123–1128 (1998). doi:10.1016/S0896-6273(00)80629-7 Medline

10. B. J. Wiltgen, R. A. Brown, L. E. Talton, A. J. Silva, New circuits for old memories: The role of the neocortex in consolidation. *Neuron* **44**, 101–108 (2004). doi:10.1016/j.neuron.2004.09.015 Medline

11. P. W. Frankland, B. Bontempi, The organization of recent and remote memories. *Nat. Rev. Neurosci.* **6**, 119–130 (2005). doi:10.1038/nrn1607 Medline

12. A. R. Preston, H. Eichenbaum, Interplay of hippocampus and prefrontal cortex in memory. *Curr. Biol.* **23**, R764–R773 (2013). doi:10.1016/j.cub.2013.05.041 Medline

13. T. Nakashiba, D. L. Buhl, T. J. McHugh, S. Tonegawa, Hippocampal CA3 output is crucial for ripple-associated reactivation and consolidation of memory. *Neuron* **62**, 781–787 (2009). doi:10.1016/j.neuron.2009.05.013 Medline

14. E. Lesburguères, O. L. Gobbo, S. Alaux-Cantin, A. Hambucken, P. Trifilieff, B. Bontempi, Early tagging of cortical networks is required for the formation of enduring associative memory. *Science* **331**, 924–928 (2011). doi:10.1126/science.1196164 Medline

15. M. Zelikowsky, S. Bissiere, M. S. Fanselow, Contextual fear memories formed in the absence of the dorsal hippocampus decay across time. *J. Neurosci.* **32**, 3393–3397 (2012). doi:10.1523/JNEUROSCI.4339-11.2012 Medline

16. L. G. Reijmers, B. L. Perkins, N. Matsuo, M. Mayford, Localization of a stable neural correlate of associative memory. *Science* **317**, 1230–1233 (2007). doi:10.1126/science.1143839 Medline

17. X. Liu, S. Ramirez, P. T. Pang, C. B. Puryear, A. Govindarajan, K. Deisseroth, S. Tonegawa, Optogenetic stimulation of a hippocampal engram activates fear memory recall. *Nature* **484**, 381–385 (2012). Medline

18. S. Tonegawa, X. Liu, S. Ramirez, R. Redondo, Memory engram cells have come of age. *Neuron* **87**, 918–931 (2015). doi:10.1016/j.neuron.2015.08.002 Medline

19. T. Kitamura, M. Pignatelli, J. Suh, K. Kohara, A. Yoshiki, K. Abe, S. Tonegawa, Island cells control temporal association memory. *Science* **343**, 896–901 (2014). doi:10.1126/science.1244634 Medline

20. L. Ye, W. E. Allen, K. R. Thompson, Q. Tian, B. Hsueh, C. Ramakrishnan, A.-C. Wang, J. H. Jennings, A. Adhikari, C. H. Halpern, I. B. Witten, A. L. Barth, L. Luo, J. A. McNab, K. Deisseroth, Wiring and molecular features of prefrontal ensembles representing distinct experiences. *Cell* **165**, 1776–1788 (2016). doi:10.1016/j.cell.2016.05.010 Medline

21. K. Deisseroth, Optogenetics: 10 years of microbial opsins in neuroscience. *Nat. Neurosci.* **18**, 1213–1225 (2015). doi:10.1038/nn.4091 Medline

22. Y. Ziv, L. D. Burns, E. D. Cocker, E. O. Hamel, K. K. Ghosh, L. J. Kitch, A. El Gamal, M. J. Schnitzer, Long-term dynamics of CA1 hippocampal place codes. *Nat. Neurosci.* **16**, 264–266 (2013). doi:10.1038/nn.3329 Medline

23. G. Sürmeli, D. C. Marcu, C. McClure, D. L. F. Garden, H. Pastoll, M. F. Nolan, Molecularly defined circuitry reveals input-output segregation in deep layers of the medial entorhinal cortex. *Neuron* **88**, 1040–1053 (2015). doi:10.1016/j.neuron.2015.10.041 Medline

24. T. J. Ryan, D. S. Roy, M. Pignatelli, A. Arons, S. Tonegawa, Engram cells retain memory under retrograde amnesia. *Science* **348**, 1007–1013 (2015). doi:10.1126/science.aaa5542 Medline

25. A. Hayashi-Takagi, S. Yagishita, M. Nakamura, F. Shirai, Y. I. Wu, A. L. Loshbaugh, B. Kuhlman, K. M. Hahn, H. Kasai, Labelling and optical erasure of synaptic memory traces in the motor cortex. *Nature* **525**, 333–338 (2015). doi:10.1038/nature15257 Medline

26. D. S. Roy, A. Arons, T. I. Mitchell, M. Pignatelli, T. J. Ryan, S. Tonegawa, Memory retrieval by activating engram cells in mouse models of early Alzheimer's disease. *Nature* **531**, 508–512 (2016). doi:10.1038/nature17172 Medline

27. T. Kitamura, C. Sun, J. Martin, L. J. Kitch, M. J. Schnitzer, S. Tonegawa, Entorhinal cortical ocean cells encode specific contexts and drive context-specific fear memory. *Neuron* **87**, 1317–1331 (2015). doi:10.1016/j.neuron.2015.08.036 Medline

28. B. A. Pellman, J. J. Kim, What can ethobehavioral studies tell us about the brain's fear system? *Trends Neurosci.* **39**, 420–431 (2016). doi:10.1016/j.tins.2016.04.001 Medline

29. K. K. Tayler, K. Z. Tanaka, L. G. Reijmers, B. J. Wiltgen, Reactivation of neural ensembles during the retrieval of recent and remote memory. *Curr. Biol.* **23**, 99–106 (2013). doi:10.1016/j.cub.2012.11.019 Medline

30. S. Maren, G. Aharonov, M. S. Fanselow, Retrograde abolition of conditional fear after excitotoxic lesions in the basolateral amygdala of rats: Absence of a temporal gradient. *Behav. Neurosci.* **110**, 718–726 (1996). doi:10.1037/0735-7044.110.4.718 Medline

31. F. H. Do-Monte, K. Quiñones-Laracuente, G. J. Quirk, A temporal shift in the circuits mediating retrieval of fear memory. *Nature* **519**, 460–463 (2015). doi:10.1038/nature14030 Medline

32. C. A. Denny, M. A. Kheirbek, E. L. Alba, K. F. Tanaka, R. A. Brachman, K. B. Laughman, N. K. Tomm, G. F. Turi, A. Losonczy, R. Hen, Hippocampal memory traces are differentially modulated by experience, time, and adult neurogenesis. *Neuron* **83**, 189–201 (2014). doi:10.1016/j.neuron.2014.05.018 Medline

33. T. Kitamura, Y. Saitoh, N. Takashima, A. Murayama, Y. Niibori, H. Ageta, M. Sekiguchi, H. Sugiyama, K. Inokuchi, Adult neurogenesis modulates the hippocampus-dependent period of associative fear memory. *Cell* **139**, 814–827 (2009). doi:10.1016/j.cell.2009.10.020 Medline

34. T. Tumbar, G. Guasch, V. Greco, C. Blanpain, W. E. Lowry, M. Rendl, E. Fuchs, Defining the epithelial stem cell niche in skin. *Science* **303**, 359–363 (2004). doi:10.1126/science.1092436 Medline

35. T. Okuyama, T. Kitamura, D. S. Roy, S. Itohara, S. Tonegawa, Ventral CA1 neurons store social memory. *Science* **353**, 1536–1541 (2016). doi:10.1126/science.aaf7003 Medline

36. K. Miyamichi, F. Amat, F. Moussavi, C. Wang, I. Wickersham, N. R. Wall, H. Taniguchi, B. Tasic, Z. J. Huang, Z. He, E. M. Callaway, M. A. Horowitz, L. Luo, Cortical representations of olfactory input by trans-synaptic tracing. *Nature* **472**, 191–196 (2011). doi:10.1038/nature09714 Medline

37. S. Ramirez, X. Liu, P.-A. Lin, J. Suh, M. Pignatelli, R. L. Redondo, T. J. Ryan, S. Tonegawa, Creating a false memory in the hippocampus. *Science* **341**, 387–391 (2013). doi:10.1126/science.1239073 Medline

38. S. Ramirez, X. Liu, C. J. MacDonald, A. Moffa, J. Zhou, R. L. Redondo, S. Tonegawa, Activating positive memory engrams suppresses depression-like behaviour. *Nature* **522**, 335–339 (2015). doi:10.1038/nature14514 Medline

39. C. R. Yu, J. Power, G. Barnea, S. O'Donnell, H. E. V. Brown, J. Osborne, R. Axel, J. A. Gogos, Spontaneous neural activity is required for the establishment and maintenance of the olfactory sensory map. *Neuron* **42**, 553–566 (2004). doi:10.1016/S0896-6273(04)00224-7 Medline

40. J. Hirrlinger, A. Scheller, P. G. Hirrlinger, B. Kellert, W. Tang, M. C. Wehr, S. Goebbels, A. Reichenbach, R. Sprengel, M. J. Rossner, F. Kirchhoff, Split-Cre complementation indicates coincident activity of different genes in vivo. *PLOS ONE* **4**, e4286 (2009). doi:10.1371/journal.pone.0004286 Medline

41. Y. Shima, K. Sugino, C. M. Hempel, M. Shima, P. Taneja, J. B. Bullis, S. Mehta, C. Lois, S. B. Nelson, A Mammalian enhancer trap resource for discovering and manipulating neuronal cell types. *eLife* **5**, e13503 (2016). doi:10.7554/eLife.13503 Medline

42. I. R. Wickersham, S. Finke, K. K. Conzelmann, E. M. Callaway, Retrograde neuronal tracing with a deletion-mutant rabies virus. *Nat. Methods* **4**, 47–49 (2007). doi:10.1038/nmeth999 Medline

43. K. Kohara, M. Pignatelli, A. J. Rivest, H.-Y. Jung, T. Kitamura, J. Suh, D. Frank, K. Kajikawa, N. Mise, Y. Obata, I. R. Wickersham, S. Tonegawa, Cell type–specific genetic and optogenetic tools reveal hippocampal CA2 circuits. *Nat. Neurosci.* **17**, 269–279 (2014). doi:10.1038/nn.3614 Medline

44. K. A. Goosens, S. Maren, Contextual and auditory fear conditioning are mediated by the lateral, basal, and central amygdaloid nuclei in rats. *Learn. Mem.* **8**, 148–155 (2001). doi:10.1101/lm.37601 Medline

45. J. Kim, M. Pignatelli, S. Xu, S. Itohara, S. Tonegawa, Antagonistic negative and positive neurons of the basolateral amygdala. *Nat. Neurosci.* **19**, 1636–1646 (2016).

46. T. Kitamura, C. J. Macdonald, S. Tonegawa, Entorhinal-hippocampal neuronal circuits bridge temporally discontiguous events. *Learn. Mem.* **22**, 438–443 (2015). doi:10.1101/lm.038687.115 Medline

47. M. Yokoyama, N. Matsuo, Loss of ensemble segregation in dentate gyrus, but not in somatosensory cortex, during contextual fear memory generalization. *Front. Behav. Neurosci.* **10**, 218 (2016). doi:10.3389/fnbeh.2016.00218 Medline

48. R. L. Redondo, J. Kim, A. L. Arons, S. Ramirez, X. Liu, S. Tonegawa, Bidirectional switch of the valence associated with a hippocampal contextual memory engram. *Nature* **513**, 426–430 (2014). doi:10.1038/nature13725 Medline

49. L. Restivo, G. Vetere, B. Bontempi, M. Ammassari-Teule, The formation of recent and remote memory is associated with time-dependent formation of dendritic spines in the hippocampus and anterior cingulate cortex. *J. Neurosci.* **29**, 8206–8214 (2009). doi:10.1523/JNEUROSCI.0966-09.2009 Medline

50. L. Pinto, Y. Dan, Cell-type-specific activity in prefrontal cortex during goal-directed behavior. *Neuron* **87**, 437–450 (2015). doi:10.1016/j.neuron.2015.06.021 Medline

51. C. Sun, T. Kitamura, J. Yamamoto, J. Martin, M. Pignatelli, L. J. Kitch, M. J. Schnitzer, S. Tonegawa, Distinct speed dependence of entorhinal island and ocean cells, including respective grid cells. *Proc. Natl. Acad. Sci. U.S.A.* **112**, 9466–9471 (2015). doi:10.1073/pnas.1511668112 Medline